Molecular Cancer

RESEARCH

Open Access

GRPR-induced *FAM135A* expression promote perineural invasion in prostate cancer

Ning Zhang[1†], Xiaohao Ruan[1†], Siteng Chen[2†], Ruofan Shi[1,4†], Xiaoqun Yang[3†], Yongle Zhan[4], Stacia Chun[4], Chi Yao[4], Salida Ali[4], Brian Sze-Ho Ho[5], Ada Tsui-Lin Ng[4,5], Richard KY Lo[4,6] and Rong Na[4,5,6*]

Abstract

Perineural invasion (PNI) is an independent adverse prognostic marker for prostate cancer (PCa) metastasis. Gastrin releasing peptide receptor (*GRPR*) targeted imaging and therapeutics have entered clinical trials, while its role in PCa perineural invasion remains unclear. Here, we uncovered Family With Sequence Similarity 135 Member A （FAM135A）a dominant PNI driver activated by GRPR in PCa. First, PNI-PCa tissue showed higher neuroactive ligand-receptor interaction activity, and with *FAM135A* being the most notable marker in PNI group. Then in-vitro experiments using a co-culture system of PCa cells (including AR-positive LNCaP and AR-negative DU145/PC3) showed that FAM135A silencing abrogated tumor malignancy and neural invasion. Moreover, in vivo PCa-Sciatic nerve invasion mouse model demonstrated *FAM135A* inhibition controls tumor growth and improves motor function. Interestingly, *FAM135A* is nucleus enriched and its nuclear translocation is mediated by protein cytoplasmic-nuclear transporter *RAN*. Mechanistically, RNA-Seq and ChIP-Seq analyses identified Teneurin Transmembrane Protein 3 (*TENM3*) as a transcriptional target of nFAM135A, and *TENM3* plays an essential role in nFAM135A-induced cancer-nerve invasion. Notably, *FAM135A* is ultimately activated by Gastrin Releasing Peptide GRP and its receptor GRPR. Moreover, pharmacological GRPR inhibitor represses *FAM135A* expression via *MED15* activation. Together, we unveil *FAM135A* as an oncodriver and biomarker of PCa perineural invasion, and provide a novel strategy for PCa innervation therapeutics.

Keywords Prostate cancer, Perineural invasion, FAM135A, GRPR, RAN

Introduction

Prostate cancer (PCa) is one of the leading malignancies globally constituting 11% of all male cancer-related deaths [1]. Despite great advances of surgical interventions and radiation therapy for localized PCa, about 30% of patients eventually face recurrence and metastasis, resulting in a 5-year survival rate between 30 and 40% [2]. Androgen deprivation therapy (ADT) is the cornerstone of PCa treatment [3]. Nonetheless, the emergence of castration-resistant prostate cancer (CRPC) indicates that PCa cells are capable of proliferating in an environment with reduced androgen levels [4]. Consequently, there is an imperative need to delve deeper into the mechanisms underlying hypo-androgenic PCa.

Nervous system-cancer crosstalk is involved in tumor initiation, progression, and resistance to interventions [5–7]. With the advent of cancer neuroscience, the pivotal role of the neural microenvironment in the advancement of tumorigenesis is increasingly being recognized and is now a focal point of research interest [5, 8, 9]. Perineural invasion (PNI) is present in 17–75% of prostate

†Ning Zhang, Xiaohao Ruan, Siteng Chen, Ruofan Shi and Xiaoqun Yang contributed equally to this work.

*Correspondence:
Rong Na
yungna@hku.hk

Full list of author information is available at the end of the article

Graphical abstract

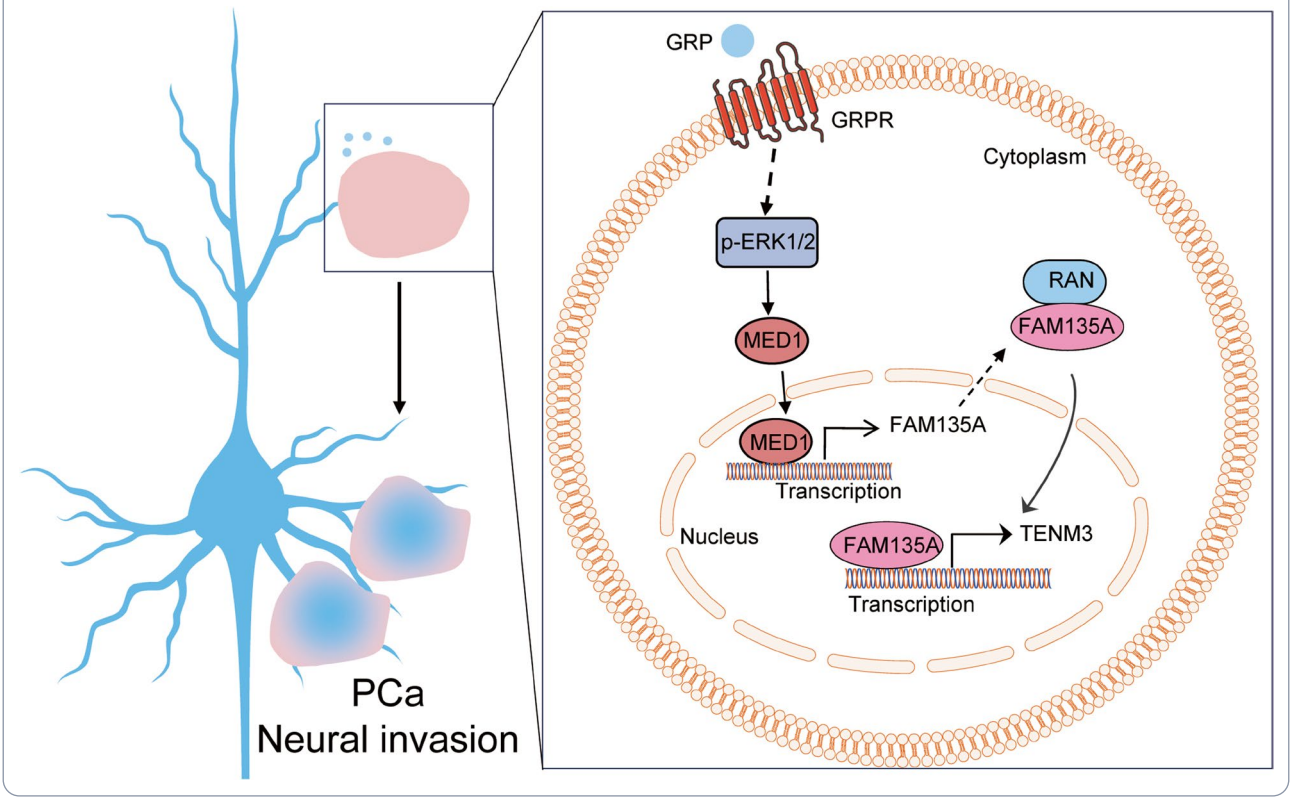

cancer patients, and is an important mechanism for cancer progression, leading to poor prognosis [10, 11]. Neurotransmitters [12, 13], neuropeptides [14, 15] and their receptors [16–18] act as progression and prognosis marker and also drive the progression of prostate cancer. Additionally, the possibility of targeting cancer-neural interactions is emerging as a promising new strategy in cancer [19, 20]. Therefore, elucidating the mechanisms underlying perineural invasion (PNI) in PCa will provide new strategies for prostate cancer treatment.

Gastrin-releasing peptide GRP is proposed to be a key itch-specific neuropeptide [21–23] and is involved in liver and kidney injury [24, 25], fear learning [26], and pulmonary fibrosis [27].Gastrin-releasing peptide receptor (GRPR) is aberrantly overexpressed in several malignant tumors [28] and used for cancer imaging and radio-therapeutics [29, 30], especially in prostate cancer [31, 32]. Notably, plasma progastrin-releasing peptide shows good performance in diagnosing lung well-differentiated neuroendocrine tumors [33]. In prostate cancer, GRPR targeted imaging and therapeutics have entered clinical trials [31, 34, 35], while its role in PCa perineural invasion remains unclear.

Here, we first conducted a comparative transcriptomic analysis of prostate cancer samples with and without perineural invasion (PNI). *FAM135A* (family with sequence similarity 135 member A) is a highly conserved gene in mammals and mainly expressed in brain, retina, and other normal tissues [36]. While mutations in *FAM135A* have been linked to pancreatic neuroendocrine tumor [37], its role in PCa remains unclear. In PNI-positive samples, *FAM135A* was found to be the most significantly upregulated gene. Further experimental data revealed that targeting *FAM135A* can control tumor growth and neural invasion, suggesting that *FAM135A* is a tumor-intrinsic driver gene. Interestingly, *FAM135A* localizes to the nucleus and *TENM3* plays an essential role in FAM135A-induced prostate cancer nerve invasion. Within this pathway, several neuroactive ligand-receptor pairs were dysregulated, including the Gastrin-Releasing Peptide Receptor (GRPR), which was significantly elevated in PNI samples. Finally, we found that *GRPR* exerts an inducing effect on *FAM135A*, and this effect is mediated by the activation of the transcription factor *MED1*. This study is the first to elucidate the key role of *FAM135A* in PCa nerve invasion and proposes a potential new therapeutic strategy for the treatment of prostate cancer nerve invasion.

Results

Identification of *FAM135A* as a neural invasive marker in prostate cancer

Perineural invasion (PNI) is an independent adverse prognostic marker for prostate cancer metastasis and prognosis [10]. However, the underlying mechanisms and key genes related to perineural invasion remain unclear. To systematically investigatePNI in prostate cancer, we first conducted comparative analysis on the data by Prueitt RL et al. [38] to obtain gene expression changes between prostate cancer(PCa) samples with PNI and Non-PNI groups. A total of 124 significantly differentially expressed mRNAs and lncRNAs were identified (Fig. 1A and B; Table 1), including 77 genes that were significantly upregulated in PNI (such as *FAM135A*, *PSCA*, *CHRM2*, and *GABRA4*) and 47 genes that were significantly downregulated (such as *GUCY2D* and *NEUROD1*). In addition to mRNAs, some lncRNAs such as RP11-286E11.2 were significantly elevated in the PNI group, while *C1QT-NF9B-AS1* was significantly reduced. Next, functional analysis of these differential genes highlighted significantly enriched pathways, such as neuroactive ligand-receptor interaction, cell adhesion molecules, and the Notch signaling pathway (Fig. 1C), suggesting that these pathways may involve in the process of PNI. Among the genes significantly enriched in Neuroactive ligand-receptor interaction, there were 10 genes (Fig. 1D), with 6 significantly elevated, including Cholinergic Receptor Muscarinic 2 (*CHRM2*), Cholinergic Receptor Muscarinic 4 (*CHRM4*), Gamma-Aminobutyric Acid Type A Receptor Subunit Alpha4 (*GABRA4*), 5-Hydroxytryptamine Receptor 2B (*HTR2B*), Vasoactive Intestinal Peptide Receptor 2 (*VIPR2*) and Gastrin-Releasing Peptide Receptor (*GRPR*), and 4 significantly reduced genes including F2R Like Trypsin Receptor 1 (*F2RL1*), Relaxin 1 (*RLN1*), Relaxin 2 (*RLN2*) and Prostaglandin E Receptor 4 (*PTGER4*). These results are consistent with previous findings that neuroactive ligand-receptor interactions mediate the innervation and progression of prostate cancer [16–18]. Among these 124 genes, *FAM135A* was the most significantly elevated gene in the PNI group (Fig. 1E). To investigate the role of *FAM135A* in PNI, we collected pathologically confirmed prostate cancer samples with PNI and without PNI and performed immunohistochemical staining for *FAM135A*. The results showed that the expression level of *FAM135A* in the PNI group was significantly higher than in the non-PNI group, suggesting a positive correlation between *FAM135A* and PNI (Fig. 1F). Quantitative analysis of IHC staining further revealed that the nuclear-to-cytoplasmic (N/C) ratio of *FAM135A* was significantly elevated in PNI-positive tumors compared to non-PNI tumors (Fig. 1G).

FAM135A promotes malignant phenotypes associated with neurological invasion in prostate cancer

To explore the role of *FAM135A* in perineural invasion (PNI) of prostate cancer, we first investigated its effects on prostate cancer cells. We first examined the impact of *FAM135A* on the malignant behavior of tumor cells. Short hairpin RNA (shRNA) targeting *FAM135A* was designed and packaged into lenti-virus to infect DU145 and PC3 cells.The knockdown efficiency was rigorously validated by qRT-PCR (Supplementary Fig. 1A) and Western blot (Supplementary Fig. 1B), confirming a significant reduction in *FAM135A* expression. Subsequently, the effects of *FAM135A* knockdown on cell proliferation, invasion, and migration were assessed. The proliferative capacity of DU145 and PC3 (Supplementary Fig. 1C) cells in the *FAM135A* knockdown group was significantly inhibited. Consistently, the number of clones formed by PCa cellswas also significantly reduced upon *FAM135A* knockdown (Supplementary Fig. 1D-1E). Moreover, the rate of tumor cell death was significantly increased (Supplementary Fig. 1F-1G) upon *FAM135A* silencing. These results indicate that *FAM135A* knockdown significantly reduces the proliferative capacity of tumor cells. Since the invasive ability of tumor cells is a crucial for their neural invasion, we further examined the invasive and migratory potential of tumor cells with *FAM135A* knockdown and found that *FAM135A* knockdown significantly reduced the invasive (Fig. 2A and B) and migratory abilities (Fig. 2C and D). To explore the role of *FAM135A* in perineural invasion of prostate cancer, we conducted a variety of in-vitro experiments to simulate the communication between tumor cells and neurons. We established a co-culture system of tumor cells and neurons (PC12) in a basement membrane matrix, where prostate cancer tumor cells PC3 and DU145 were seeded within the matrix, and PC3 and DU145 tumor cells were plated around them (tumor cells were labeled with red and PC12 labeled green dye) (Fig. 2E). By quantifying the number and proportion of tumor cells surrounding PC12, we compared the effect of *FAM135A* knockdown on the invasiveness of tumor cells into neurons. The results revealed that *FAM135A* knockdown significantly reduced the number of cells surrounding the PC12 synapses after 48h of co-culture (Fig. 2F and G), suggesting an impaired ability, rather than a mere delay, in tumor cell invasion towards nerves under these experimental conditions. This in-vitro finding suggests that *FAM135A* can markedly decrease the invasiveness of tumor cells towards nerves. Moreover, we constructed a co-culture system of Dorsal Root Ganglion (DRG) and tumor cells in the basement membrane matrix (Fig. 2H), and quantified the number of DRG invaded by tumor cells. Consistently, we found that the number of *FAM135A*-silenced cells around the DRG was significantly reduced (Fig. 2I

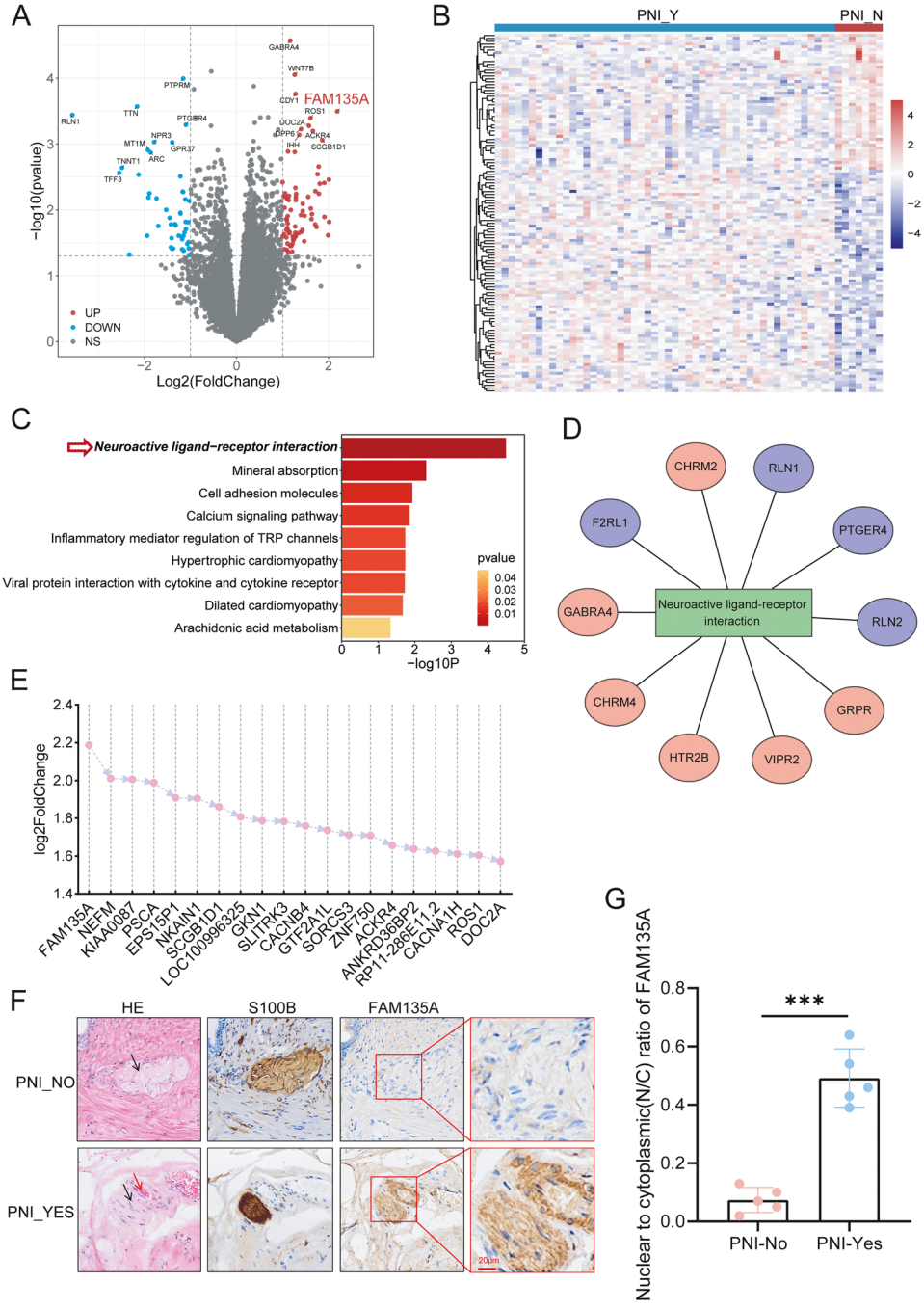

Fig. 1 *FAM135A* is a perineural invasion marker in prostate cancer. **A**. Transcriptomic analysis (based on data from GSE10779 of PNI and non-PNI prostate cancer samples identified significantly differentially expressed genes using an FDR-adjusted *p*-value < 0.05 and a |log2 fold change| >1 **B**. Heatmap of significantly differentially expressed genes comparing PNI to non-PNI. Rows are Z-score normalized. **C**. Bar plot showing the top significantly enriched KEGG pathways from the functional analysis of the differentially expressed gene set in (A). Pathway enrichment analysis was performed using the DAVID bioinformatics database. The y-axis indicates the -log10 (*P*-value) **D**. The 10 most significantly dysregulated genes belonging to the "Neuroactive ligand-receptor interaction" KEGG pathway. **E**. Bar plot of the top 20 most significantly upregulated genes in the PNI group, ranked by log2 fold change **F**. Representative immunohistochemical (IHC) staining for FAM135A in pathologically confirmed PNI versus non-PNI prostate cancer samples. Arrows indicate: yellow, tumor cells; black, nerves. Dual IHC staining for S100 (a Schwann cell marker) and FAM135A was performed on consecutive/serial sections to unequivocally identify PNI, as described in the Methods. Scale bar: 20 μm. **G**. Quantitative analysis of the nuclear-to-cytoplasmic (N/C) ratio of FAM135A IHC staining in PNI-No and PNI-Yes samples. Data are presented as mean ± SD; $^{**}P < 0.01$ (Student's t-test) ** $P < 0.01$;

Table 1 Clinical characteristics of prostate cancer patients for immunohistochemical validation

No.	Group	Age	Gleason Score	WHO/ISUP	Tumor Area Ratio
P1	PNI	71	7	3	50%
P2	PNI	70	7	2	20%
P3	PNI	71	7	2	25%
P4	PNI	71	7	2	10%
P5	PNI	69	7	3	80%
P6	Non-PNI	69	7	2	15%
P7	Non-PNI	66	7	2	25%
P8	Non-PNI	69	7	2	2%
P9	Non-PNI	68	7	2	3%
P34	Non-PNI	72	7	2	20%

and J). These in-vitro experimental results indicate that *FAM135A* knockdown significantly inhibits its interaction with nerves, and that inhibiting *FAM135A* has potential therapeutic effects in suppressing PNI.

To systematically evaluate the effects of *FAM135A* on the interaction between tumor cells and neurons, we injected *FAM135A*-silenced prostate cancer cells and control cells into the sciatic nerves of mice model, and subsequently assessed changes in tumor volume and the motor function (Fig. 3A). The results revealed that the tumor volume in the sciatic nerve of mice injected with *FAM135A*-silenced cells was significantly smaller than that of the control group (Fig. 3B), indicating that *FAM135A* silencing inhibits tumor growth along nerve fibers. Furthermore, compared to the control group mice (uninjected mice), mice injected with control tumor cells exhibited significantly reduced motor ability, whereas mice injected with *FAM135A*-silenced tumor cells showed less motor impairment (Fig. 3C and D), suggesting that *FAM135A* silencing can mitigate the impact of tumor cell invasion on nerve motor function. To further evaluate the status of tumor nerve invasion, we performed hematoxylin and eosin (H&E) staining and Ki67 staining on the tumor tissues, and found that the degree of tumor perineural invasion in the *FAM135A*-silenced group was significantly decreased (Fig. 3E). To confirm the sustained knockdown of *FAM135A* in the sciatic nerve tumors at the experimental endpoint, we performed immunohistochemical (IHC) staining for *FAM135A* on the harvested tumor tissues. The results demonstrated that *FAM135A* expression remained significantly lower in the sh*FAM135A* group compared to the control group (Fig. 3F and G), validating that the observed phenotypic effects were due to persistent silencing of *FAM135A*. Collectively, these in vitro and in vivo results demonstrate that *FAM135A* silencing significantly inhibits the malignant behavior of PCa cells, suggesting that *FAM135A* inhibition may serve as a therapeutic target for suppressing tumor progression. Additionally, the interaction between tumor cells and neurons not only plays a crucial role in tumor advancement but also affects neural function.

RAN mediates the nuclear translocation of *FAM135A*

Next, we attempt to analyze the mechanism of *FAM135A* in PCa cells. Immunofluorescence staining reveals that *FAM135A* is localized in the cell nucleus (THPA database) (Suplemetary Fig. 2A). Further, we examined the localization of *FAM135A* in prostate cancer cells PC3 and DU145 by immunofluorescence and found that *FAM135A* is localized in both the cytoplasm and the nucleus (Fig. 4A), suggesting that *FAM135A* may have a potential transcriptional regulatory role. We sought to identify crucial regulators underlying nuclear translocation of *FAM135A*. Studies showed that Nuclear-Cytoplasmic Transport is a key process in tumor progression [39]. Therefore, we performed co-immunoprecipitation (Co-IP) on *FAM135A* and identified binding proteins by mass spectrometry (MS). The complete list of interacting proteins is provided as Supplementary Table 1. Among these binding proteins, three were involved in nucleocytoplasmic transport including SRRM1, RNPS1, and RAN (Fig. 4B and Supplementary Fig. 2B). Since *RAN* can promote tumor progression by inducing abnormal nuclear translocation of proteins [40], we focused on whether *RAN* mediates the nuclear translocation of *FAM135A*. First, we performed immunoprecipitation of RAN and discovered by Western Blot that *RAN* indeed binds to *FAM135A* (Fig. 4C). Subsequently, we silenced the *RAN* (Fig. 4D) and used a nuclear-cytoplasmic separation kit to detect the distribution of FAM135A in the nucleus (nFAM135A) and cytoplasm (cFAM135A) after *RAN* silencing. The results showed that *RAN* silencing significantly reduced the abundance of nuclear *FAM135A* (nFAM135A), with GAPDH as a positive control for the cytoplasm and PCNA for the nucleus, while the expression abundance in the cytoplasm (cFAM135A) was not significantly affected (Fig. 4E). All three proteins are known to shuttle between the nucleus and cytoplasm. Next, we individually silenced *SRRM1* and *RNPS1* in PC3 and DU145 cells (Supplementary Fig. 2C-F). Nuclear-cytoplasmic fractionation followed by Western blotting was then performed. Knockdown of *SRRM1* or *RNPS1* had no substantial effect on thenuclear levels of *FAM135A* (Supplementary Fig. 2G). *RAN* can mediate the nuclear retention of *FAM135A*. Finally, we performed immunofluorescence for *RAN* and *FAM135A* and found co-localization of *RAN* and *FAM135A* (Fig. 4G). This indicates that among these binding partners, *RAN* is the primary regulator responsible for facilitating the nuclear translocation of *FAM135A*.

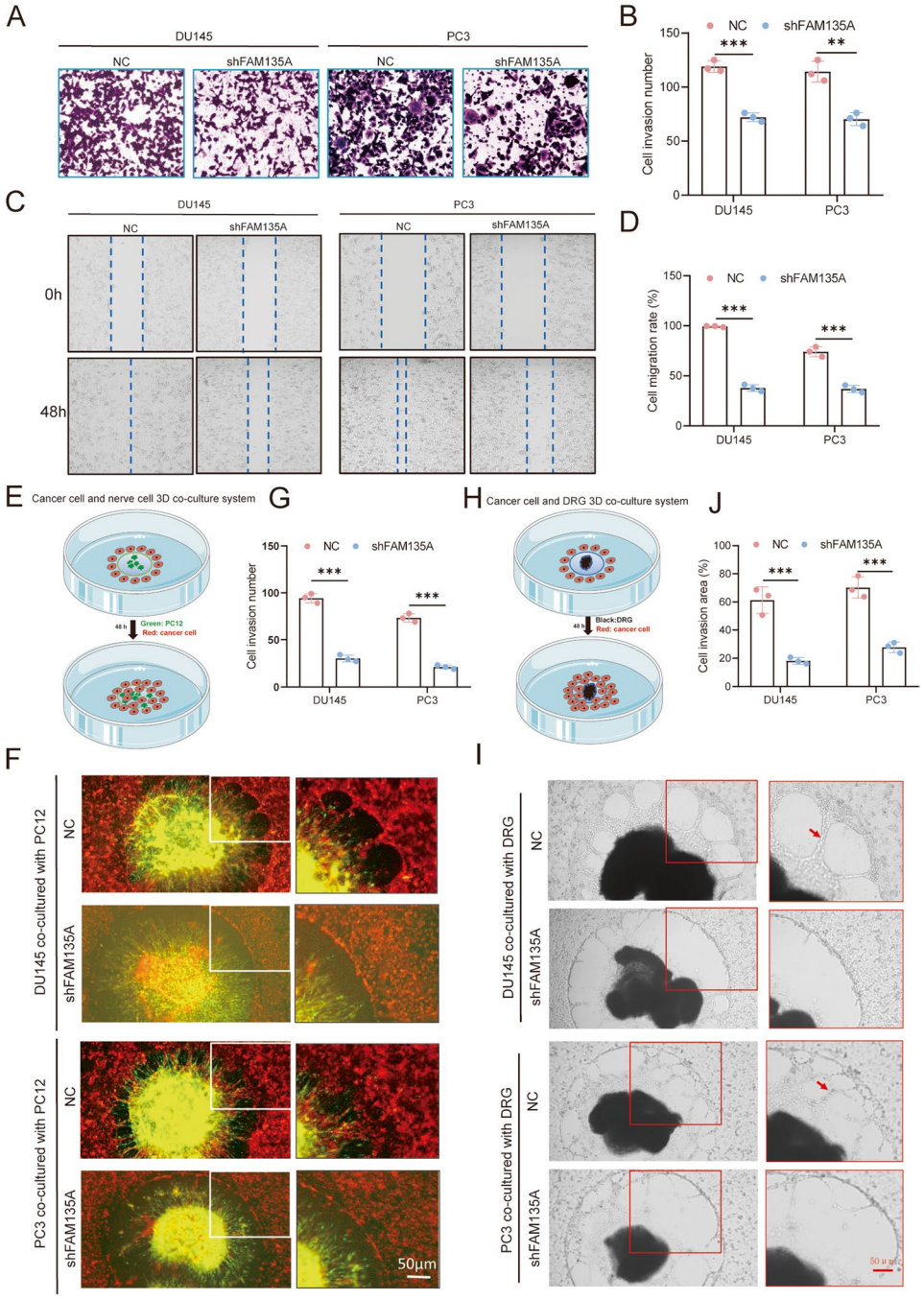

Fig. 2 Silencing of *FAM135A* gene significantly inhibits the invasion of prostate cancer cells and reduces the ability of tumoral neural invasion.**A**-**B**: Transwell invasion assays reveal that silencing *FAM135A* reduces cellular invasiveness; **C**-**D**: Wound healing scratch assays demonstrate a significant decrease in the migratory ability of *FAM135A*-silenced cells E. Schematic diagram illustrating the co-culture model of tumor cells with neuronal Matrigel; **F**-**G**. Fluorescence microscopy showing the change in the number and extent of tumor cell invasion of neurites after *FAM135A* silencing following a 48h co-culture (scale bar: 50 μm); **H**. Schematic diagram illustrating the co-culture model of tumor cells with dorsal root ganglion (DRG) neurons; **I**-**J**. Bright-field images showing the morphological and degree changes of tumor cell invasion of DRG under bright-field microscopy after 48h of co-culture (scale bar: 50 μm) ** $P < 0.01$; *** $P < 0.001$;

Integrated RNA-Seq and ChIP-Seq analysis identifies *TENM3* as a novel transcriptional target of *FAM135A*

To elucidate the regulatory mechanisms of *FAM135A* in prostate cancer cells, we performed RNA-Seq on *FAM135A*-silenced and control PC3 and DU145 cells, and compared the significantly differentially expressed genes (DEGs) between them. A total of 1026 (PC3, Fig. 5A and Supplementary Fig. 3A) and 212 (DU145,

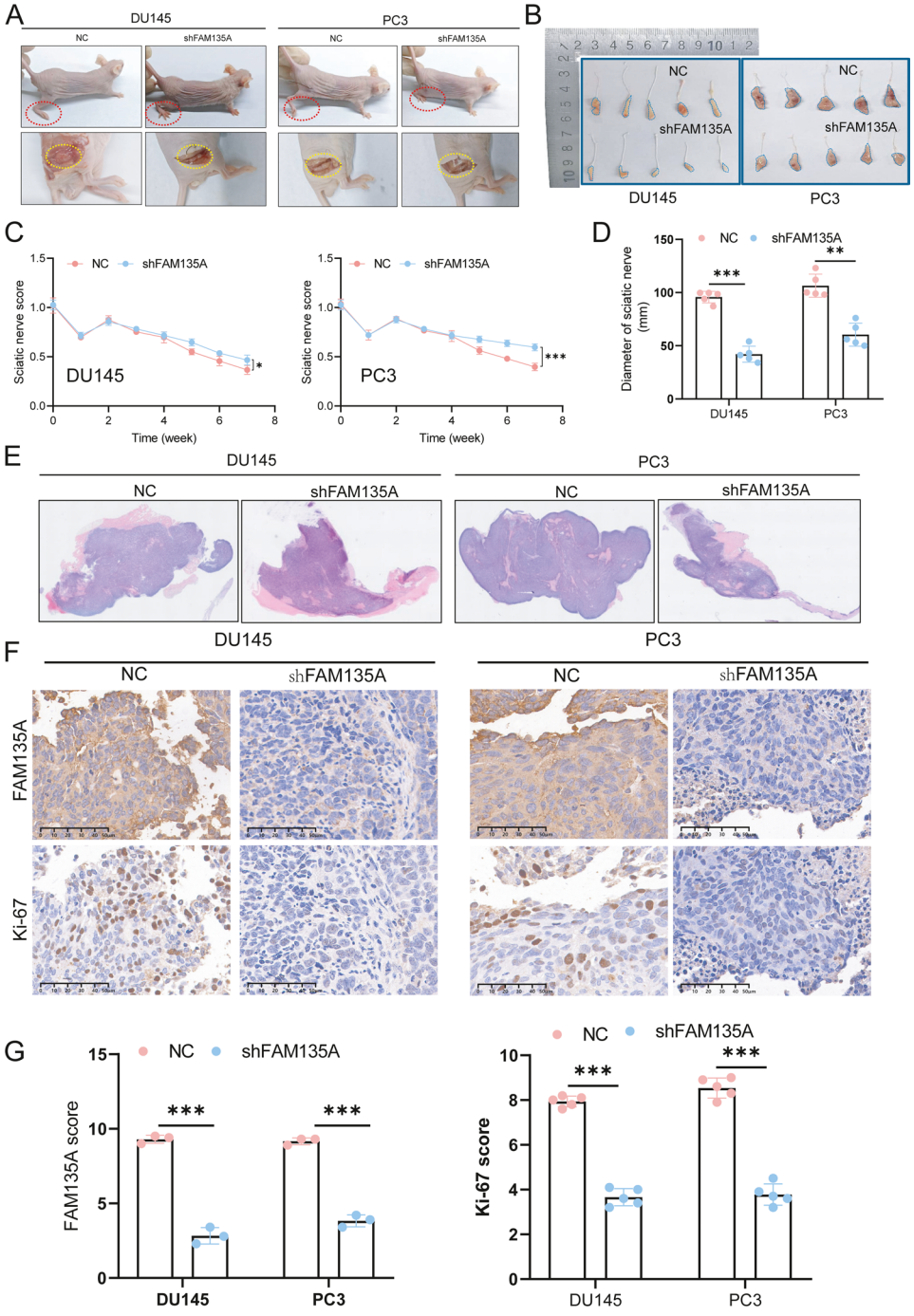

Fig. 3 Mouse sciatic nerve model demonstrates that *FAM135A* silencing can inhibit tumor growth and improve neuromuscular motor function.**A**. Injection of tumor cells into the mouse sciatic nerve results in motor dysfunction in the mice; **B**. Dissection of the sciatic nerve tumor in mice reveals a reduction in both volume and longitudinal migration along the nerve; **C**. Silencing of *FAM135A* significantly improves the sciatic nerve motor score in mice; **D**. Compared to the control group, the diameter of the sciatic nerve is significantly reduced in the *FAM135A*-silenced group; **E**. H&E staining shows morphological changes in tumor tissue within the sciatic nerve; **F**-**G**: Tumor tissue is stained with the proliferation marker Ki67, and the results show that *FAM135A* silencing significantly reduces Ki67 staining scores $^{*}P < 0.05$; $^{**}P < 0.01$; $^{***}P < 0.001$;

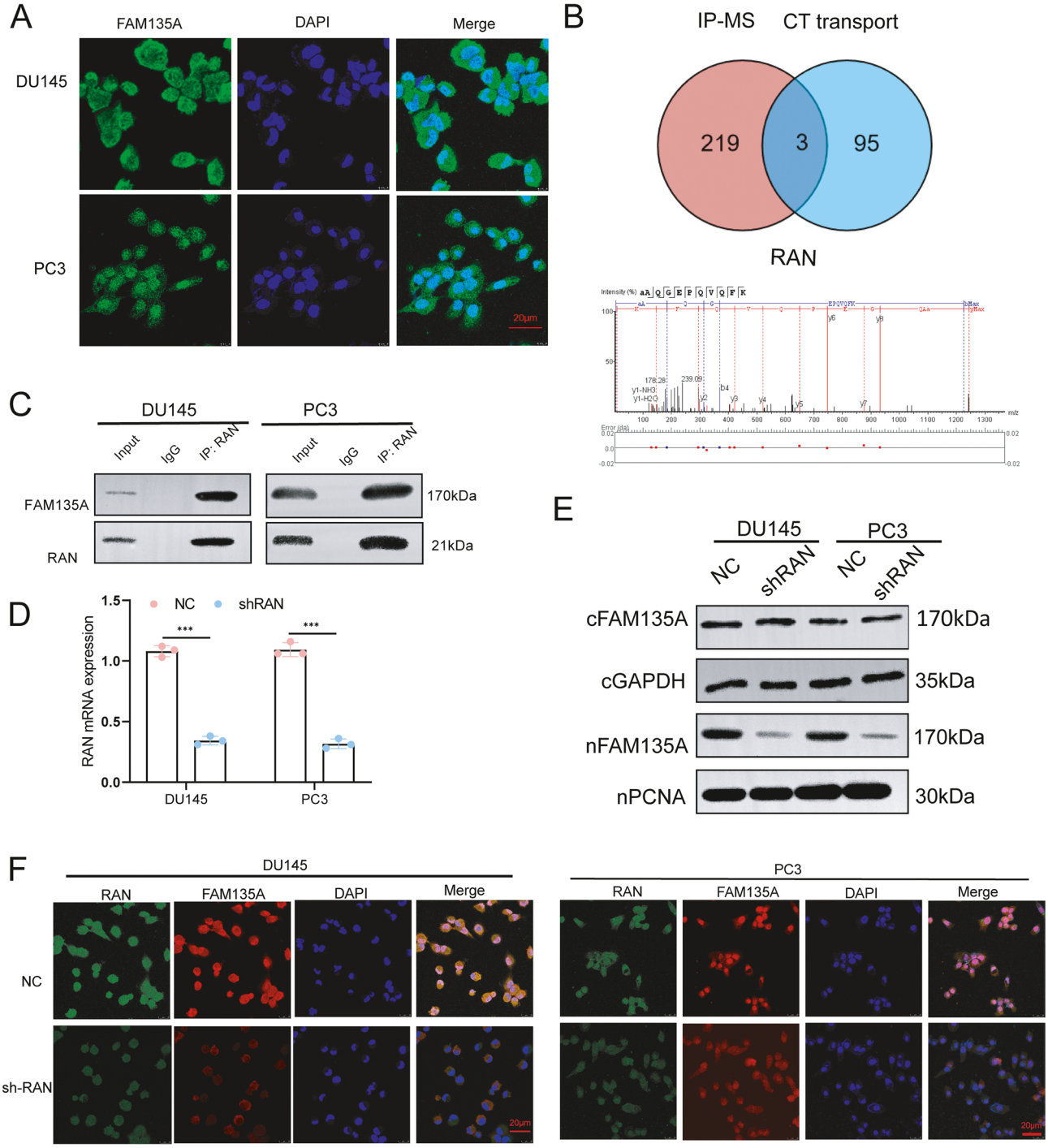

Fig. 4 *RAN* mediates the nuclear translocation of *FAM135A*.**A**. Immunofluorescence staining shows that FAM135A is localized in the nuclei of PCa cells (scale bar: 20 μm); **B**. Flag tag was constructed for FAM135A, and potential binding proteins were identified through co-immunoprecipitation, with a focus on proteins involved in cytoplasmic-nuclear transport, resulting in the identification of three proteins; SRRM1, RRNPS1, and RAN; **C**. Co-immunoprecipitation of RAN was performed, and the interaction between FAM135A and RAN was confirmed by Western blot (WB); **D**. The efficiency of *RAN* silencing was verified after *RAN* was silenced; **E**. Nuclear-cytoplasmic fractionation was performed in cell lines where *RAN* was silenced, and protein abundance changes in both the cytoplasm and nucleus were detected; **G**. In DU145 and PC3 cells, immunofluorescence was used to detect the co-localization of RAN with FAM135A (scale bar: 20 μm) *** $P < 0.001$;

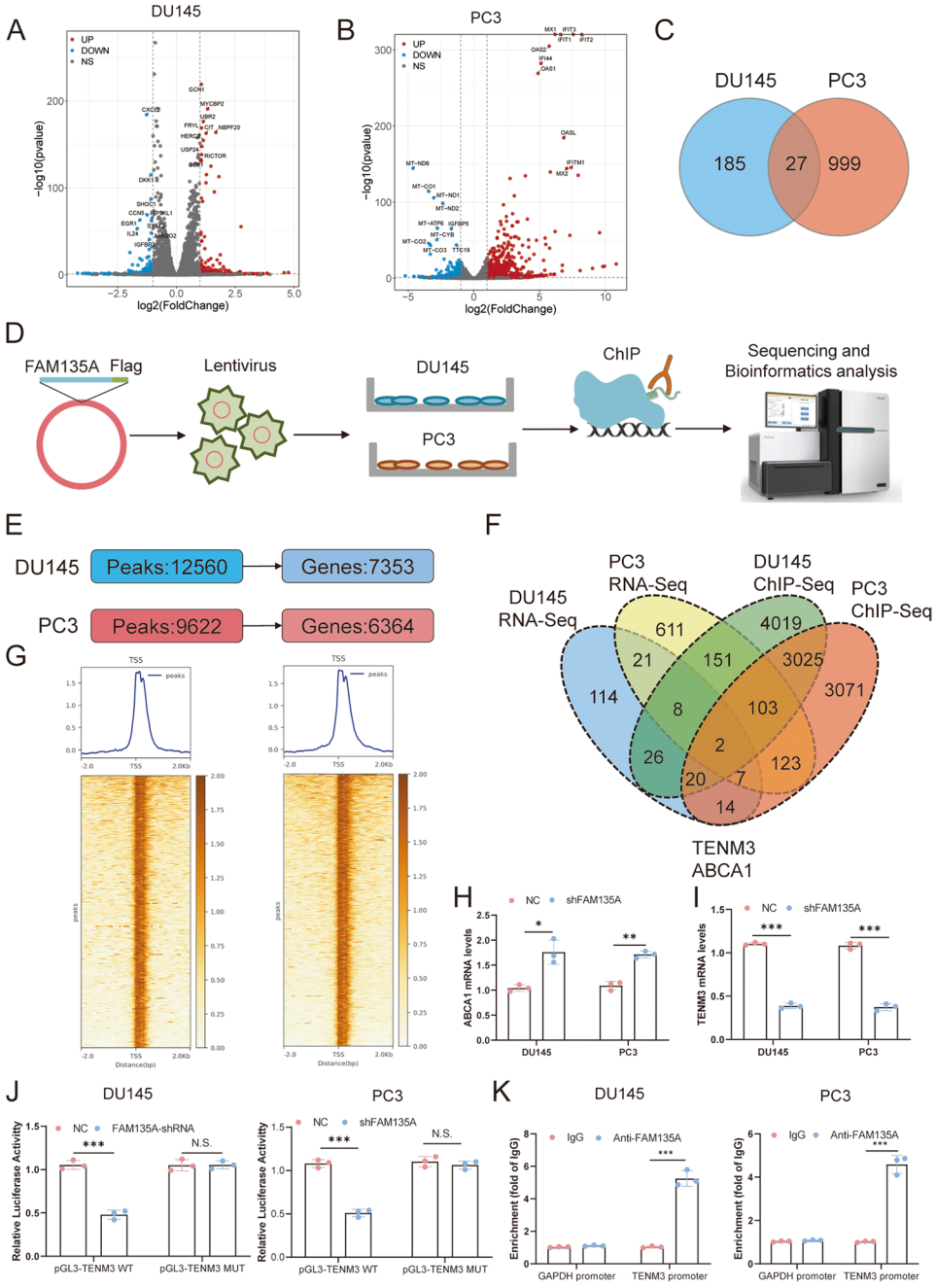

Fig. 5 RNA-Seq and ChIP-Seq identify novel transcriptional targets of *FAM135A*.**A**-**B**. Transcriptomic analysis of significantly differentially expressed genes in *FAM135A*-silenced DU145 and PC3 cells using an FDR-adjusted p-value < 0.05 and a |log2 fold change| >1; **C**. Combined analysis of differential genes from both cell lines identified 27 common differentially expressed genes; **D**. Construction of *FAM135A* with a Flag tag and identification of potential target genes through ChIP-Seq; **E**. ChIP-Seq analysis identified FAM135A binding peaks in DU145 and PC3 cells, and annotated corresponding genes for the binding peaks; **F**. Combined analysis of ChIP-Seq and RNA-Seq data identified two common genes, *TENM3* and *ABCA1*; **G**. Heatmap showing the distribution of FAM135A binding peaks near the transcription start site (TSS) of genes **H**. Silencing of *FAM135A* significantly reduced the mRNA levels of *ABCA1*; **I**. Silencing of *FAM135A* significantly reduced the mRNA levels of *TENM3*; **J**. Luciferase reporter gene assay found that mutation of the promoter sequence abolished the binding activity of FAM135A on the *TENM3* promoter; **K**. ChIP-PCR experiments verified the binding of FAM135A to the *TENM3* promoter *** $P < 0.001$;

Fig. 5B and Supplementary Fig. 3B) significantly DEGs were identified in the two cell lines, respectively (Supplementary Table 2). We then conducted a joint analysis of the significantly DEGs in both cell lines, identifying 27 commonly significantly DEGs (Fig. 5C and Supplementary Fig. 3C). Among these, 23 genes were upregulated upon *FAM135A* silencing (such as *ABCA1*), while 4 genes were downregulated (such as *TENM3*), suggesting that these genes may be potential target genes of *FAM135A*.

To further determine the transcriptional regulatory mechanisms of *FAM135A* in prostate cancer PNI, we constructed a Flag-fused system for *FAM135A* and performed chromatin immunoprecipitation sequencing (ChIP-Seq) to reveal its transcriptional regulation of target genes (Fig. 5D). Peak calling was performed on PC3 and DU145 cells, and the identified Peaks were annotated with genes. A total of 12,560 peaks were identified in DU145, annotating to 7,353 genes, while 9,622 peaks were identified in PC3, annotating to 6,364 genes (Fig. 5E). Notably, the proportion of peaks located in the promoter region was 13.94% (DU145) and 13.5% (PC3), such as that of the *ID2* gene (Fig. 5F and Supplementary Fig. 3D). By integrating the genes identified from RNA-Seq and ChIP-Seq, we found that among the 27 commonly significantly differentially expressed genes, 2 genes were also identified in the ChIP-Seq *TENM3 a*nd *ABCA1* (Fig. 5F). A heat map illustrates the distribution of FAM135A binding peaks in the region near the gene TSS locus (transcription start site) (Fig. 5G).

Next, we silenced the *FAM135A* gene and detected the expression changes of *ABCA1* and *TENM3* using quantitative real-time PCR (qRT-PCR). The results showed that *FAM135A* silencing significantly increased the expression of *ABCA1* (Fig. 5H) and reduced the expression of *TENM3* mRNA (Fig. 5I), suggesting that *FAM135A* can induce *TENM3* expression. Since *ABCA1* is a well-characterized tumor suppressor in prostate cancer that inhibits progression by regulating cholesterol metabolism, and its expression increased following *FAM135A* silencing [41, 42]. Given the well acknowledged role of *ABCA1* in prostate cancer, we focused on *TENM3* for subsequent analysis. *TENM3* is known to be involved in the regulation of neuronal development and neuroblastoma tumorigenesis [43], leading us to hypothesize that *TENM3* may be a potential target gene induced by FAM135A in prostate cancer PNI. Finally, to further validate the transcriptional regulatory effect of *FAM135A* on *TENM3*, we conducted a dual-luciferase reporter gene assay and validated the effect of *FAM135A* on *TENM3* transcriptional activity (Fig. 5J). Subsequently, we verified the binding of FAM135A to the *TENM3* promoter using ChIP-PCR and found a significant enrichment of FAM135A binding peaks in the promoter region of *TENM3* (Fig. 5K). Collectively, our results showed that FAM135A can activate *TENM3* transcription, thereby promoting its expression.

FAM135A induces perineural invasion in prostate cancer by transcriptional activation of *TENM3*

Subsequently, to explore the role of *TENM3* in *FAM135A*-induced perineural invasion (PNI) of prostate cancer, we first performed immunohistochemically (IHC) staining for *TENM3* in PNI and non-PNI prostate cancer tissues. The results revealed significant overexpression of *TENM3* in PNI tissues (Fig. 6A and B). Next, we focused on the function of *TENM3* in prostate cancer PNI. The knockdown efficiency was rigorously validated by qRT-PCR (Supplementary Fig. 4A) and Western blot (Supplementary Fig. 4B), confirming significant reduction of *TENM3* expression. Subsequently, the effects of *TENM3* knockdown on PNI were assessed. In transwell co-culture(Fig. 6C and D) and DRG-PCa cell co-culture models, we observed that *TENM3* knockdown significantly reduced the area of tumor cell invasion into nerves (Fig. 6E and F). Furthermore, in the in vivo sciatic nerve tumor implantation model, *TENM3* knockdown significantly inhibited the tumor volume of the sciatic nerve (Fig. 6G), and the functional scoring of mouse sciatic nerve also significantly improved (Fig. 6H), suggesting that *TENM3* knockdown can also amellorate nerve function impairmenr. Subsequently, we performed hematoxylin and eosin (H&E) staining (Fig. 6I) and Ki67 IHC staining on the tumor tissues (Fig. 6J and K), and found that *TENM3* knockdown reduced the Ki67 score. These results indicate that *TENM3* knockdown can significantly inhibit the process of prostate cancer PNI.

We then explored the role of *TENM3* in *FAM135A*-mediated promotion of perineural invasion (PNI). We overexpressed *TENM3* in DU145 and PC3 cells with stable *FAM135A* knockdown shows the validation of *TENM3* overexpression in this background (**Supplementary Fig. 5A**). We then observed the results in the transwell co-culture and DRG-PCa cell co-culture model. In the transwell co-culture(Fig. 7A and B)and DRG-PCa cell co-culture model (Fig. 7C and D), the overexpression of *TENM3* partially restored the reduction in the area of tumor cell invasion into nerves caused by *FAM135A* silencing. Consistent with the results from the DRG-PCa cell co-culture model, in the sciatic nerve tumor implantation model conducted with DU145 cells (Fig. 7E), we also found that the overexpression of *TENM3* partially reversed the inhibitory effect of *FAM135A* silencing on tumor growth (Fig. 7F), and the functional scoring of mouse sciatic nerve significantly improved (Fig. 7G). Furthermore, histological staining (Fig. 7H) and Ki67 immunohistochemical (IHC) staining also confirmed the rescuing effect of *TENM3* overexpression on *FAM135A*

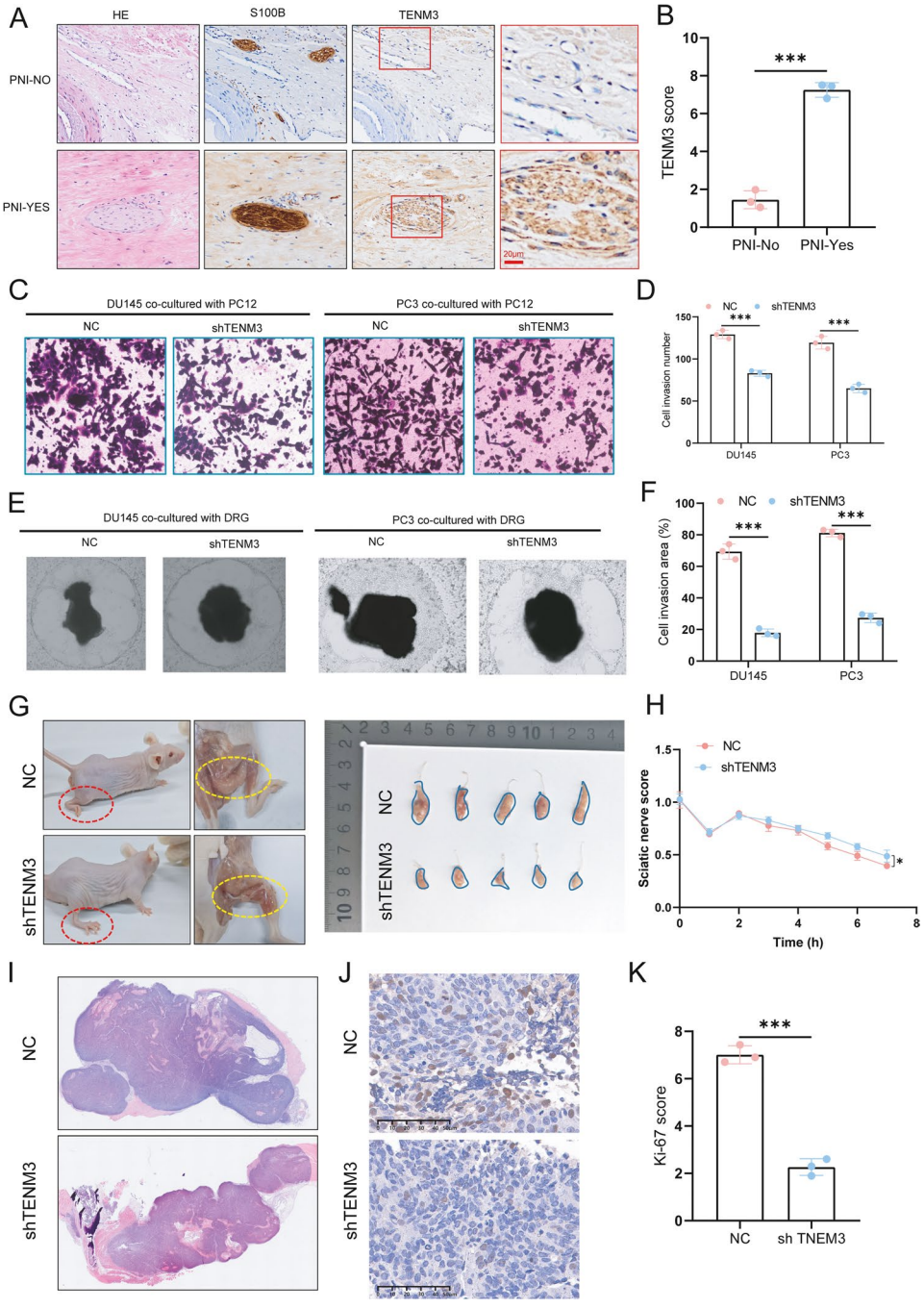

Fig. 6 *TENM3* is significantly overexpressed in PNI prostate cancer and promotes cancer to neural invasion.**A**-**B**. Immunohistochemistry shows that *TENM3* is significantly overexpressed in PNI-positive prostate cancer samples (scale bar: 20 μm); **C**-**D**. Silencing of *TENM3* and co-culturing with PC3 neuronal cells using Transwell assays reveal that *TENM3* significantly inhibits tumor cell invasion towards neurons; **E**-**F**. In the tumor cell-DRG co-culture model, silencing of *TENM3* significantly inhibits tumor cell invasion towards DRG neurons after 48 h of co-culture; **G**-**H**. Injection of *TENM3*-silenced tumor cells into the mouse sciatic nerve shows that *TENM3* silencing significantly reduces tumor size and improves neurologic function; **I**. H&E staining of tumor tissue from NC and *FAM135A*-silenced tumors; **J**-**K**. IHC staining shows that *FAM135A* silencing significantly inhibits the expression of Ki67 (scale bar: 60 μm) **P* < 0.05; *** *P* < 0.001;

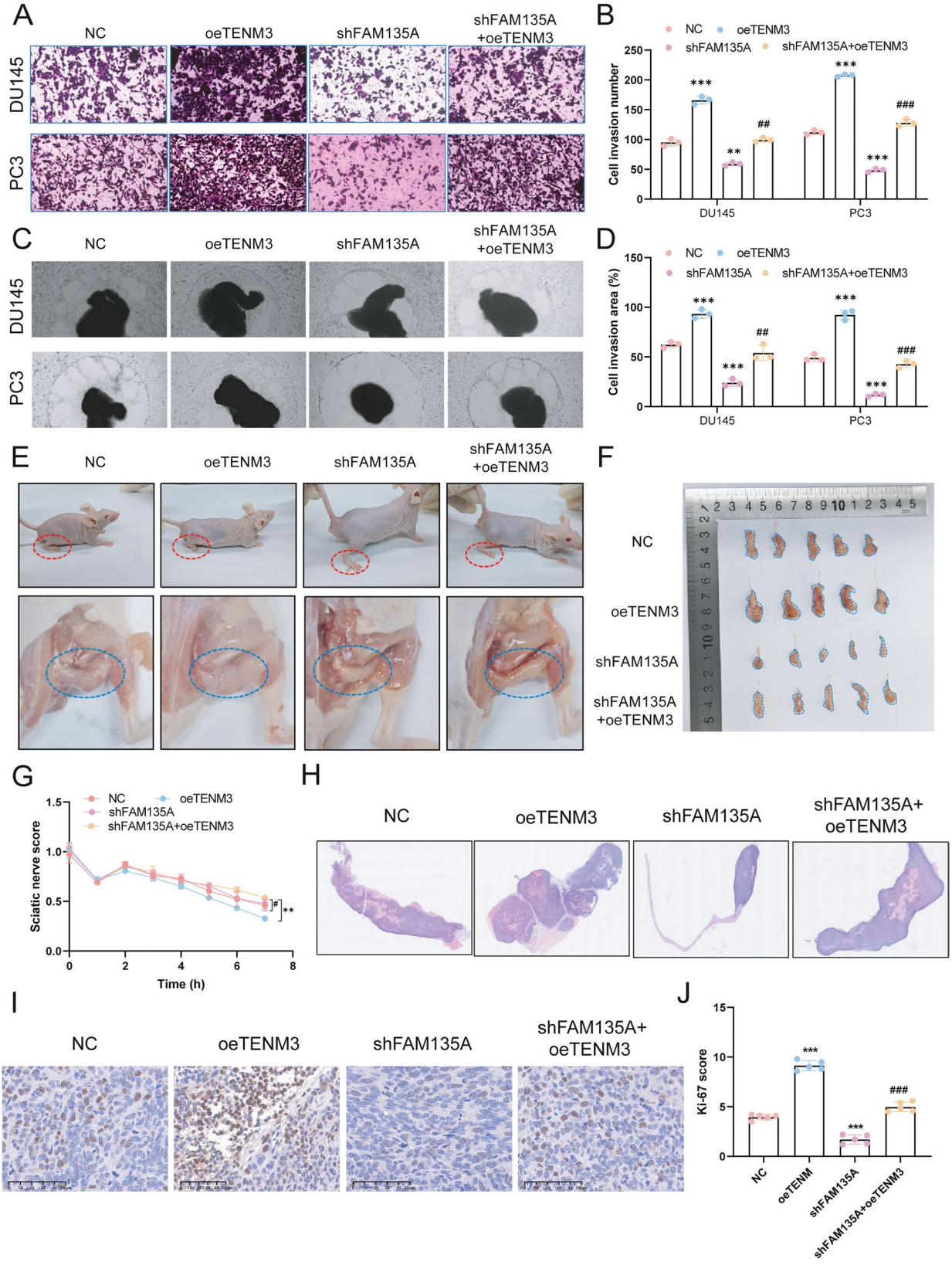

Fig. 7 (See legend on next page.)

(See figure on previous page.)

Fig. 7 *FAM135A* promotes neural invasion of cancer through *TENM3*.**A**-**B**. Overexpression of *TENM3* in *FAM135A*-silenced tumor cells, followed by co-culturing with PC3 neuronal cells using Transwell assays, reveals that *TENM3* rescues the inhibitory effect of *FAM135A* on tumor cell invasion towards neurons; **C**-**D**. Overexpression of *TENM3* in *FAM135A*-silenced tumor cells, followed by the tumor cell-DRG co-culture model, shows that *TENM3* rescues the inhibitory effect of *FAM135A* on tumor cell invasion towards DRG; **E**-**F**. Injection of tumor cells overexpressing *TENM3* and silenced for *FAM135A* into the mouse sciatic nerve reveals that *TENM3* rescues the inhibitory effects of *FAM135A* on tumor growth and improvement of neurologic function; **G**. Sciatic nerve motor scores for groups overexpressing *TENM3*, silenced for *FAM135A*, and co-treated with *TENM3* overexpression and *FAM135A* silencing; **H**. H&E staining of tumor tissue from groups overexpressing *TENM3*, silenced for *FAM135A*, and co-treated with *TENM3* overexpression and *FAM135A* silencing; **I**-**J**. Ki67 staining of tumor tissue from groups overexpressing *TENM3*, silenced for *FAM135A*, and co-treated with *TENM3* overexpression and *FAM135A* silencing (scale bar: 60 μm); ** Indicates comparison with the NC group*, *$P < 0.05$; **$P < 0.01$; ***$P < 0.001$; # indicates comparison with the sh*FAM135A* group, #$P < 0.05$; ##$P < 0.01$; ###$P < 0.001$

silencing (Fig. 7I and J). The above results suggest that *TENM3* plays a key role in *FAM135A* -induced PNI in prostate cancer.

FAM135A is induced by the expression of the neuroligand Gastrin-Releasing Peptide Receptor (GRPR)

Finally, since *FAM135A* is significantly overexpressed in PNI samples, and PNI is likely mediated by Neuroactive ligand-receptor interaction, we considered what ligand-receptor pair might induce the high expression of *FAM135A* in PNI. Therefore, we first analyzed the expression of 10 Neuroactive ligands and receptors in relation to the expression of *FAM135A*, and found that only the *GRPR* (Gastrin-Releasing Peptide Receptor) showed a significantly strong positive correlation with *FAM135A* (Pearson $r = 0.3788$, $p < 0.001$) (Fig. 8A and Supplementary Fig. 6), suggesting that GRPR plays an inducing role in *FAM135A*. Studies have found that Gastrin-releasing peptide receptors are frequently overexpressed in human prostate cancer, and radiolabeled GRPR affinity ligands have shown promise for in-vivo imaging of prostate cancer with PET [31, 34, 44]. Therefore, to explore whether GRPR regulates *FAM135A*, we first interfered with the expression of *GRPR* and found that *GRPR* silencing significantly inhibited the expression of *FAM135A* (Fig. 8B). Then, we treated prostate cancer cell lines with the commercial non-peptide GRPR antagonist PD176252 [28], and found that, similar to RNA interference, PD176252 treatment significantly inhibited the expression of *FAM135A* (Fig. 8C). Furthermore, we treated prostate cancer cell lines with human recombinant GRP (hrGRP), and found that the expression of *FAM135A* increased with the concentration of hrGRP treatment (Fig. 8D).Previous studies have reported that gastrin-releasing peptide receptor induces ERK phosphorylation [45] and ERK phosphorylates and drives *MED1* expression and activation [46]. WB analysis confirmed that *GRPR* knockdown in DU145 and PC3 cells significantly inhibited the levels of phosphorylated ERK (p-ERK) and phosphorylated MED1 (p-MED1) (Fig. 8E and F). Finally, to explore the specific mechanism by which *GRPR* induces *FAM135A*, we analyzed the transcription factors that regulate *FAM135A* in prostate cancer and found that MED1 had a strong binding peak in the promoter region of the *FAM135A* gene (Fig. 8G). We confirmed through luciferase experiments that MED1 targets the promoter region of *FAM135A*, and silencing *MED1* inhibits the transcriptional activity of *FAM135A* (Fig. 8H and I). Therefore, the above results indicate that *FAM135A* is regulated by GRPR, and these activities are related to the transcriptional activation of MED1 in the p-ERK/p-MED1 signaling pathway.

The *GRPR-FAM135A-TENM3* axis is functionally conserved in AR-positive prostate cancer cells

Given the central role of the androgen receptor (AR) in the majority of prostate cancer cases and its reported relevance to PNI, we sought to determine whether the *GRPR-FAM135A-TENM3* signaling axis operates in AR-positive prostate cancer cells. We validated our key findings in LNCaP, a classic AR-positive cell line. First, we confirmed that the regulatory relationship between *GRPR* and *FAM135A* is preserved. Treatment of LNCaP cells with the GRPR antagonist PD176252 and *GRPR* shRNA significantly suppressed *FAM135A* expression, while the agonist hrGRP increased it (Fig. 9A and C). Next, we efficiently silenced *FAM135A* in LNCaP cells (Fig. 9D). Similar to the results in AR-negative cells, *FAM135A* knockdown in LNCaP cells led to a marked reduction in cell invasion capacity in Transwell assays (Fig. 9E and F), LNCaP co-culture PC12 (Fig. 9G and H) and significantly impaired tumor cell invasion towards DRG neurons in the co-culture model (Fig. 9I and J). Furthermore, qRT-PCR analysis confirmed that *TENM3* mRNA levels were decreased upon *FAM135A* silencing (Fig. 9K), indicating that the transcriptional regulation of *TENM3* by nuclear *FAM135A* is also maintained in an AR-positive context. These data suggest that the *GRPR-FAM135A-TENM3* axis may function in parallel to the canonical AR signaling pathway in the tested models.

Discussion

Perineural invasion (PNI) in prostate cancer is a common pathological phenomenon and poor prognostic marker, but its key molecular mechanisms largely unexplored [10, 47]. Neuropeptides, neurotransmitters, and their receptors and regulators play a crucial role in PNI of prostate cancer, possibly by making tumor cells more

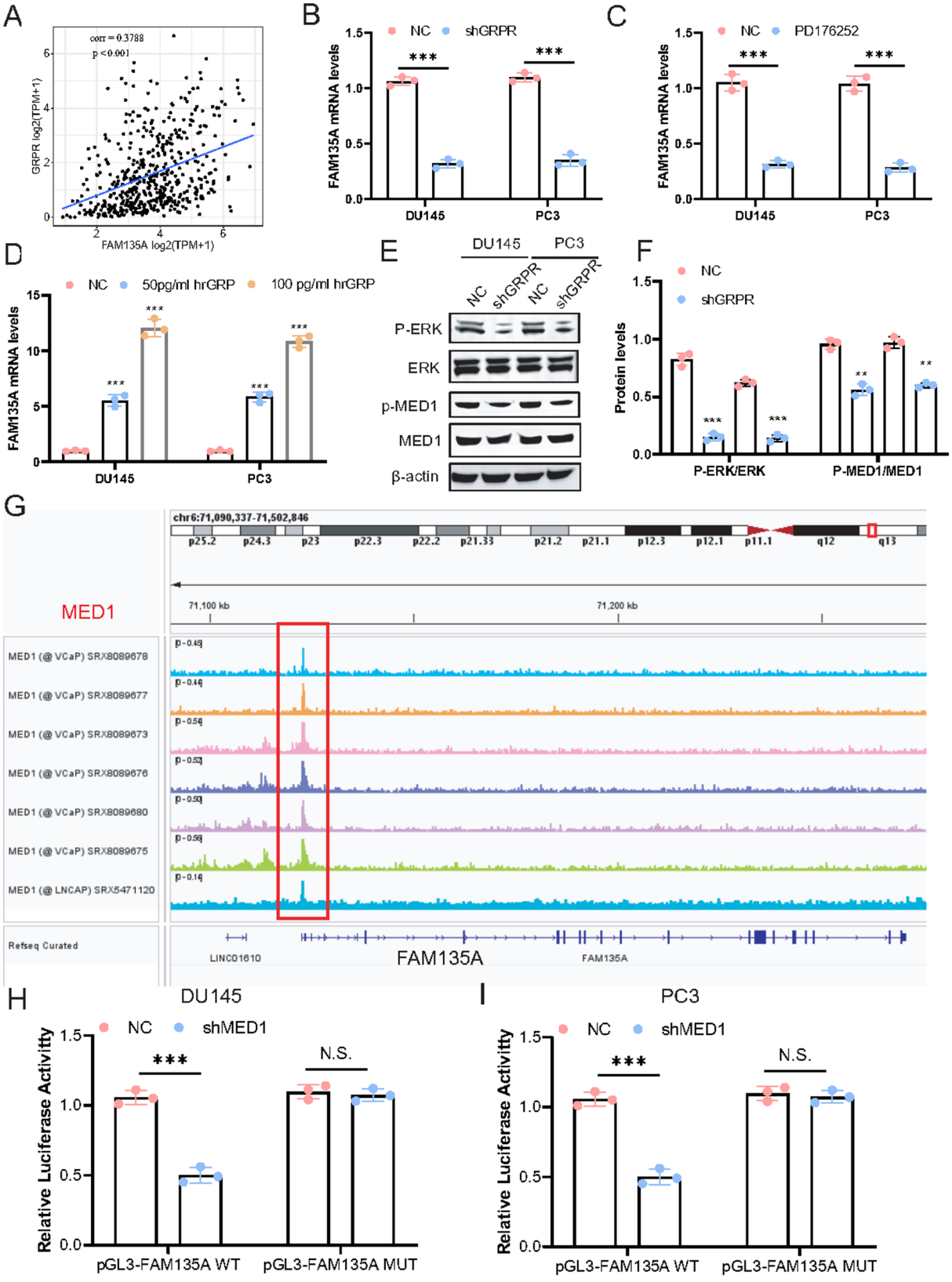

Fig. 8 (See legend on next page.)

(See figure on previous page.)

Fig. 8 *FAM135A* transcriptionally activates the expression of *TENM3;* **A**. Data analysis shows a significant positive correlation between *GRPR* and *FAM135A*(Pearson $r = 0.3788$, $p < 0.001$); **B**. Silencing of *GRPR* leads to a decrease in *FAM135A* expression; **C**. An inhibitor of *GRPR* significantly reduces *FAM135A* expression; **D**. *FAM135A* expression increases with increasing concentrations of hrGRP treatment; **E**-**F**. Levels of p-ERK and p-MED1 are reduced after *GRPR* silencing; **G**. MED1 has binding peaks upstream of the *FAM135A* promoter; **H**-**I**. Luciferase reporter gene assays show that MED1 can activate *FAM135A* transcription ** $P < 0.01$; *** $P < 0.001$;

"chemotactic" towards nerves [12, 13, 15, 48]. Therefore, this study aims to uncover the pathological phenomenon of PNI, focusing on the angle of *FAM135A* driving tumor invasion of nerves to reveal related mechanisms, providing a new perspective on the tumor-intrinsic mechanisms driven by the neuropeptide GRPR in PNI.

The first key finding of this study is the differential expression of neuro-ligand receptors such as *GRPR* in prostate cancer samples with PNI. Interestingly, it is noteworthy that, in addition to the high expression of neuro-ligand receptors like *GRPR* and *VIPR2* in the PNI group, the expression of acetylcholine receptors *CHRM2* and *CHRM4*, GABA receptor *GABRA4*, and serotonin receptor *HTR2B* is also elevated in the PNI group, while the expression of *RLN1* and *RLN2* is significantly reduced. This suggests that the occurrence of the PNI phenomenon may be driven synergistically by neurotransmitters and neuropeptides. Previous studies have also explored and revealed their key roles in tumor-neural interactions or tumor invasion of nerves from the perspective of neurotransmitters and neuropeptides [12–15]. *GRPR*, for instance, has been reported in prostate cancer, but the key downstream targets remain to be discovered.

FAM135A is a highly conserved protein across multiple species. In our research, we discovered that targeting and silencing *FAM135A* not only blocked the malignant phenotypes such as proliferation and invasion in prostate cancer tumor cells. More importantly, *FAM135A* knockdown also inhibited the phenomenon of tumor invasion of nerves. These results were confirmed in our in vitro tumor cell-neuron and tumor cell-DRG co-culture models using Matrigel, and more importantly, they were validated in a mouse model of sciatic nerve tumor that mimics neuro-oncological interactions. These functional results indicate that targeting *FAM135A* may be a key target for inhibiting PNI and progression in prostate cancer.

Additionally, *FAM135A* has been found to be localized in nucleus. Based on this observation, we further explored the nuclear translocation mechanism of *FAM135A* and identified RAN (RAS-related nuclear protein) as the key protein that mediates the nuclear translocation of *FAM135A*. RAN is a small GTP-binding protein belonging to the RAS superfamily, which is essential for the translocation of RNA and proteins through the nuclear pore complex. Interestingly, previous studies have found that RAN is an androgen receptor (AR) co-activator [49]. Our research found that when RAN is inhibited, the nuclear localization signal of *FAM135A* is significantly reduced, indicating that *RAN* is a necessary gene for mediating the nuclear translocation of *FAM135A*. Therefore, our results also found that *RAN* seems to be involved in the process of prostate cancer nerve invasion in an AR-independent manner.

Upon discovering that RAN drives the nuclear import of *FAM135A*, we hypothesized that FAM135A might function as a transcriptional regulator. We then performed ChIP-Seq to identify binding peaks in PCa cells following *FAM135A* silencing and found that *FAM135A* indeed globally reshapes the transcriptional profile of PCa cells, supporting the conjecture that FAM135A acts as a transcriptional regulator. Further, by combining RNA-Seq results, we identified *TENM3* and *ABCA1* as genes detected by both RNA-Seq and ChIP-Seq. *ABCA1* is a tumor-suppressor in prostate cancer and represses tumor progression by regulating cholesterol metabolism, its expression are increased following *FAM135A* silencing [41, 42]. Given the well acknowledged role of *ABCA1* in prostate cancer, we focused on *TENM3* for subsequent analysis. *TENM3*(Teneurin-3) has previously been recognized as a factor in neural functions like topographic circuit assembly [50] and visual circuitry [51]. In cancer, genetic *TENM3-ALK* fusion is involved in *ALK* activation in neuroblastoma [43], and *TENM3* mutations predicts poor survival in esophageal cancer [52]. We confirmed that it also plays a function like *FAM135A* in promoting PNI in PCa tumor cells. Therefore, the identification of the intracellular *FAM135A-TENM3* PNI-driving signaling axis provides a new link in the molecular mechanisms underlying the pathological phenomenon of PNI.

An interesting observation from our integrated omics analysis is that while FAM135A binds to the promoter regions of approximately 7,000–8,000 genes, only a small fraction of these (0.2%, represented by *TENM3* and *ABCA1*) exhibited consistent transcriptional changes upon *FAM135A* knockdown. This phenomenon is not uncommon in transcriptional regulation studies and can be attributed to several biological mechanisms. First, not all transcription factor binding events are functionally consequential for transcription; some may represent 'poised' or 'pioneer' binding that requires additional co-factors or specific cellular contexts to activate or repress gene expression [53]. Second, the binding of FAM135A to a promoter might serve a structural or chromatin-organizing role that does not directly alter the transcription rate of the immediate target gene. Third, cellular

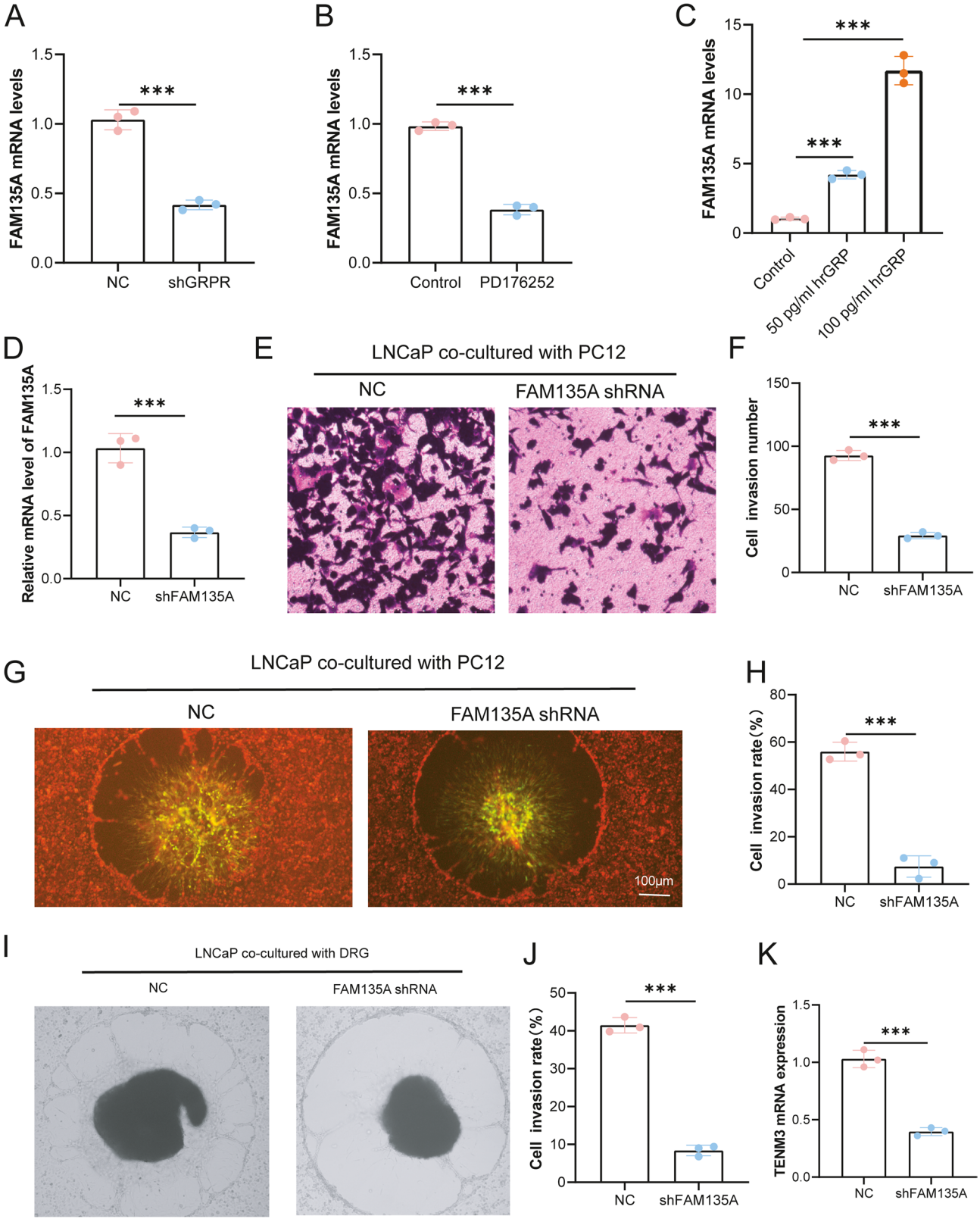

Fig. 9 (See legend on next page.)

(See figure on previous page.)

Fig. 9 The *GRPR-FAM135A-TENM3* axis is functionally conserved in AR-positive prostate cancer cells.**A** *FAM135A* mRNA levels in LNCaP cells treated with the GRPR antagonist PD176252. **B** *FAM135A* mRNA levels in LNCaP cells after *GRPR* knockdown. **C** *FAM135A* mRNA levels in LNCaP cells treated with increasing concentrations of the GRPR agonist human recombinant GRP (hrGRP). **D** Validation of *FAM135A* knockdown efficiency in LNCaP cells by qRT-PCR. **E**-**F** Transwell invasion assays showing that *FAM135A* knockdown inhibits the invasive capacity of LNCaP cells. Quantitative analysis (**E**) and representative images (**F**) are shown. **G**-**H** Tumor cell-PC12 neuron co-culture assays demonstrating that *FAM135A* knockdown impairs LNCaP cell invasion towards neurons. Quantitative analysis (**G**) and representative fluorescence images (**H**) are shown (Scale bar: 100 μm). Red: tumor cells; Green: PC12 neurons. (**I**-**J**) Tumor cell-DRG co-culture assays confirming the impaired neural invasion of *FAM135A*-silenced LNCaP cells. Quantitative analysis (**I**) and representative bright-field images (**J**) are shown. (**K**) qRT-PCR analysis showing downregulation of *TENM3* mRNA upon *FAM135A* silencing in LNCaP cells *Data are presented as mean ± SD; *$p < 0.05$, **$p < 0.01$, **$p < 0.001$

compensatory mechanisms and redundancy in transcriptional networks can buffer the effect of losing a single regulator on most of its bound genes, with only the most sensitive nodes showing significant expression changes [54]. The fact that we successfully identified and validated *TENM3* from this small, high-confidence overlap underscores its critical role as a key functional effector downstream of nuclear *FAM135A* in driving PNI.

We discovered that within the neural ligand-dominated microenvironment of PCa neural invasion, GRPR plays a key role in inducing the transcription of *FAM135A*, a role that can be activated by GRP or inhibited by GRPR inhibitors. This finding provides a potential new strategy for targeting PNI and tumor-neural interactions, possibly offering new indications for the application of GRPR antagonists or inhibitors. Additionally, the mechanism by which GRPR induces the transcriptional expression of *FAM135A* may be mediated by the transcription factor MED1, which is proven to directly mediate the transcriptional activation of *FAM135A*. Furthermore, since p-ERK is implicated in the regulatory effects of GRPR on the *MED1-FAM135A* transcriptional axis, inhibitors targeting p-ERK may also have the potential to inhibit PNI in prostate cancer. These inhibitors of GRPR and p-ERK will be explored in future research endeavors.

While our data demonstrate that prostate cancer cells respond to exogenous GRP, the physiological and pathological source of GRP in the prostate tumor microenvironment warrants further investigation. Potential sources could include: (1) neuroendocrine cells that can be present in prostate cancer, especially in advanced or treatment-resistant cases; (2) autocrine or paracrine secretion from a subset of prostate cancer cells themselves, a phenomenon described for other neuropeptides in cancer; or (3) innervating or stromal neurons within the tumor microenvironment, aligning with the concept of cancer neuroscience. Future studies using spatially resolved techniques will be crucial to map the precise source of GRP in prostate tumors with PNI.

Furthermore, to address the clinical relevance of our findings beyond AR-independent contexts, we validated the *GRPR-FAM135A-TENM3* axis in AR-positive LNCaP cells. The conserved functionality of this pathway in both AR-negative and AR-positive models suggests that it may represent a common mechanism driving PNI, potentially operating in parallel to or independently of the canonical AR signaling. This significantly broadens the potential patient population that could benefit from therapeutic strategies targeting this axis.

While our study establishes a crucial role for *FAM135A* in driving PNI, it is important to note a key limitation. Our functional experiments utilized shRNA-mediated knockdown, which depletes FAM135A from both the cytoplasm and nucleus. As such, the distinct contributions of nuclear FAM135A (nFAM135A) versus cytoplasmic FAM135A (cFAM135A) to the malignant phenotypes observed remain to be disentangled. Our data indicate that the nuclear translocation of FAM135A is an active process mediated by RAN, and our IHC analysis revealed a significantly higher nuclear-to-cytoplasmic ratio of FAM135A in PNI-positive tumors, strongly suggesting that the nuclear pool of FAM135A is functionally important. To definitively address this in the future, it will be essential to employ sophisticated tools such as engineered *FAM135A* mutants that are constitutively localized to either the nucleus (e.g., by adding a nuclear localization signal, NLS) or retained in the cytoplasm (e.g., by adding a nuclear export signal, NES). Such approaches will allow us to precisely dissect the specific functions of nFAM135A, particularly its transcriptional regulatory role, from the potential roles of cFAM135A. Furthermore, a more comprehensive investigation into the signaling pathways and post-translational modifications that regulate the subcellular localization of FAM135A will be a valuable direction for subsequent studies.

An important consideration arising from our study is the relationship between PNI and metastasis. Perineural invasion is recognized as a distinct pathological entity that can facilitate tumor dissemination independently of lymphatic or vascular routes. In our in vivo model, we focused on quantifying the local tumor burden along the sciatic nerve and its direct functional impact on motor performance. We did not, however, systematically assess distant metastases in organs such as the lungs or liver at the experimental endpoint. This represents a limitation of our current study. The intriguing possibility that the *GRPR-FAM135A-TENM3* axis, in addition to driving local nerve invasion, could also prime tumor cells for distant spread via the neural route warrants dedicated future investigation. Such studies would involve longer

observation periods and sensitive methods to track and detect disseminated tumor cells in distant organs and neural ganglia.

Beyond elucidating a novel mechanistic axis in PNI, our findings harbor significant translational potential for improving prostate cancer management. The robust overexpression of *FAM135A* in PNI-positive tumors, coupled with its critical role in driving neuro-invasive phenotypes, nominates it as a promising biomarker for stratifying patients at higher risk for aggressive, nerve-centric disease progression. This could be particularly valuable in biopsy specimens to guide more aggressive initial therapy or for patient selection in clinical trials. More importantly, our data suggest that therapeutic targeting of the *GRPR-FAM135A-TENM3* axis could directly counter PNI.

In conclusion, our study for the first time elucidates the neuro-oncological interaction mechanisms underlying neural invasion in prostate cancer and identifies the key gene *FAM135A* that drives tumor invasion of nerves. *FAM135A* is activated by the *GRPR-MED1* signaling axis and, upon nuclear import mediated by RAN, induces the transcriptional activation of *TENM3*, thereby facilitating the invasion of nerves by tumor cells. The research provides a novel strategy for targeting the *GRPR-FAM135A* axis and developing inhibitors to combat perineural invasion (PNI) and neural invasion in prostate cancer.

Materials and methods

Patients and tissues specimens

Resected specimens were collected from patients with primary Prostate cancer from Shanghai Ruijin hospital. The phenomenon of perineural Invasion (PNI) are confirmed by at least two pathologists.

Analysis of public transcriptomic data

The transcriptomic dataset from Prueitt RL et al. [38] (GEO accession: GSE10779), generated using the Affymetrix Human Genome U133 Plus 2.0 Array platform, was downloaded from the Gene Expression Omnibus (GEO) database. The raw CEL files were processed and normalized using the justRMA function in the affy R package with default parameters for background correction and quantile normalization. Probe sets were mapped to gene symbols using the corresponding platform annotation file. Differential expression analysis between PNI-positive and PNI-negative prostate cancer samples was performed using the limma R package. Genes with an absolute log2 fold change (log2FC) > 1 and a false discovery rate (FDR)-adjusted p-value < 0.05 were considered statistically significantly differentially expressed. Functional enrichment analysis of Gene Ontology (GO) terms and Kyoto Encyclopedia of Genes and Genomes (KEGG) pathways was conducted on the significant gene set using the clusterProfiler R package, with an FDR < 0.05 considered significant.

Pathological assessment of perineural invasion

The diagnosis of perineural invasion (PNI) was made according to the widely accepted standard in urological pathology, which defines PNI as the presence of tumor cells in the perineural space, involving at least one-third of the nerve's circumference [55]. All resected prostate cancer specimens were independently reviewed by two experienced genitourinary pathologists who were blinded to the clinical and molecular data. Any discrepant cases were discussed at a multi-head microscope to reach a consensus. To unequivocally confirm the presence of tumor cells within nerves and to avoid potential misinterpretation with Schwann cells, we performed dual immunohistochemical (IHC) staining for S100 (a marker for Schwann cells) on representative sections from all PNI-positive and a subset of PNI-negative cases. A case was definitively classified as PNI-positive only when Cytokeratin-positive tumor cells were observed within the perineural space, surrounded by S100-positive Schwann cells.

Immunohistochemical (IHC) staining

To unequivocally confirm the presence of tumor cells within nerves and to avoid potential misinterpretation with Schwann cells, we performed dual immunohistochemical staining for S100 (a marker for Schwann cells) on representative sections from all PNI-positive and a subset of PNI-negative cases. A case was definitively classified as PNI-positive only when FAM135A-positive tumor cells were observed within the perineural space, surrounded by S100-positive Schwann cells. IHC staining was staining was carried out in accordance with a standardized protocol. In brief, paraffin-embedded sections were incubated at 4℃ with primary antibodies (Cell Signaling Technology, Danvers, USA). Following three washes with PBS, the sections were exposed to suitable biotinylated secondary antibodies (Cell Signaling Technology, Danvers, USA) for 1 h at room temperature. Subsequently, after another three PBS washes, the sections were visualized using DAB (3,3′-diaminobenzidine) (Sigma-Aldrich, St. Louis, USA), with hematoxylin utilized for counterstaining. The staining intensity was graded as follows: 0 = negative, 1 = weak, 2 = moderate, and 3 = strong. The scoring for positive cells was categorized as: 0 for < 1%, 1for 1–25%, 2 for 25–50%, 3 for 50–75% and 4 for > 75% positive cells. The IHC score was determined by multiplying the positive cells score by staining intensity score, resulting in the final score obtained by multiplying the intensity score by the percentage score.

Cell lines and cell culture

Human prostate cancer cells PC3, DU145, rat adrenal pheochromocytoma PC-12 and human embryonic kidney 293 T cell lines were obtained from American Type Culture Collection (ATCC). PC-3, DU145 and PC-12 cells were cultured in RPMI1640 medium containing 10% fetal bovine serum (Gibco, Thermo Fisher Scientific, Waltham, USA), and placed in a 37℃, 5% CO_2 cell culture incubator.

Stable ShRNA lentiviral transfection

FAM135A shRNA and negative control shRNA (sh NC) were inserted into GV248 lentiviral vectors (Genechem, Shanghai, China), known for their efficacy in genetic manipulation of eukaryotic cells. Lentivirus was employed to transfect prostate cancer cells, leading to the downregulation of *FAM135A* expression. The shRNAs were procured from GeneChem Co, Ltd. (Shanghai, China). Cells were then seeded in 24-well plates at a density of 1×10^4 cells per well, followed by the addition of 5 μL of lentiviral particles to each well. The culture medium was replaced with fresh complete medium after an 8-hour incubation period. Subsequently, puromycin was applied to select cells that had been successfully transfected with the viral particles. After a 3-week period, puromycin-resistant cells were isolated for further analysis.

Cell proliferation assay

Cells were cultured in 96-well plates, and a certain volume of cell suspension was added to each well. The 96-well plates were incubated in a cell incubator at 37℃ with 5% CO2. The cell counting kit-8 (CCK8, Dojindo Molecular Technologies, Kyushu, Japan) was added cell well at 24 h, 48 h, and 72 h. After addition of CCK-8, the 96-well plates cell were returned to the incubator for continued incubation for 2 h. The absorbance of each well was measured at a wavelength of 450 nm using a microplate reader (Bio-Rad Laboratories, Hercules, USA).

Colony formation assay

The colony formation assay is used to evaluate the cell proliferation ability. Cell suspension preparation: Starting from cells in the logarithmic growth phase, the cells are completely suspended in complete culture medium by enzymatic digestion and accurately counted. In each experimental group, the controlled number of cells is within the range of 500 cells/well and seeded in a 6-well plate. Continuously culture for 14 days, or until the number of cells in most individual colonies exceeds 50. During the culture process, change the culture medium every 3 days and observe the cell status. After colony formation, fix the cells with 1 mL of 4% paraformaldehyde for 15–30 min. Staining: Add 1 mL of crystal violet t (Sigma-Aldrich, St. Louis, USA) staining solution to each well, and control the staining time within 10–20 min. Wash the cells multiple times with PBS and record with photography.

Annexin V-FITC/PI flow cytometry analysis

Cell apoptosis was measured using Annexin V-FITC/PI kit (Beyotime Biotechnology, Shanghai, China). Briefly, PC-3 and DU145 cells were collected and washed with PBS after transfection. The cells were then incubated in 500 μl binding buffer for 15 min before adding 5 μl of Annexin V-FITC/PI and staining the cells for another 15 min. Finally, apoptotic cells were detected by flow cytometry analysis.

Transwell invasion assay

Following the coating of the chamber with fresh Matrigel (BD Bioscience San Hose, CA, USA), 2×10^5 cells suspended in serum-free medium was seeded in the upper well of each chamber. The lower chamber was filled with medium containing 20% FBS as a chemoattractant. After a 48 h incubation, non-migrating cells were eradicated from the filter using a cotton swab, while cells on the lower surface were fixed by methanol and stained with crystal violet. Subsequently, cells that invaded through the membrane were counted under a microscope in randomly selected high-power fields, repeated three times for accuracy.

Wound healing assay

Wound healing assay were conducted as follow: tumor cells were plated and grown to 90% confluency. A wound was created by manually scraping the cell monolayer using a pipette tip. After washing the cells once with the appropriate medium, the medium was replenished, and incubation was continued. Images of the wound were captured at specified time points.

DRG dissection and isolation

The ganglia underwent mild digestion through a sequential addition of papain and collagenase buffer. The dissociated dorsal root ganglia (DRG) were then cultured in 24-well plates at 37 °C with 5% CO2 for 24 h in Dulbecco's Modified Eagle Medium supplemented with F-12 (DMEM/F-12) medium (Gibco, Thermo Fisher Scientific, Waltham, USA). Subsequently, the cells were exposed to a culture medium containing cytarabine (ara-C, 5 ug/mL) for an additional 24 h to suppress the growth of non-neuronal cells.

Tumor cell-dorsal root ganglia (DRG) co-culture assay

The tumor cell-DRG co-culture assay was conducted in accordance with previous protocols. Briefly, DRGs were extracted from the lumbar spinal region of 8-day-old

Sprague-Dawley rats following anterior laminectomy. These excised DRGs were then positioned approximately 0.5 mm away from a cluster of carcinoma cells within growth-factor-depleted Matrigel matrix. Subsequently, neurobasal medium (Invitrogen, Thermo Fisher Scientific, Waltham, MA, USA) supplemented with 10% FBS (Gibco, Thermo Fisher Scientific, Waltham, USA), 100 U/mL penicillin (Gibco, Thermo Fisher Scientific, Waltham, USA), 100 ug/mL streptomycin (Gibco, Thermo Fisher Scientific, Waltham, USA), 0.5 mM L-glutamine (Gibco, Thermo Fisher Scientific, Waltham, USA), and 2% B-27 (Invitrogen, Thermo Fisher Scientific, Waltham, USA) was added to the wells and changed every 2 days. The co-culture was maintained for a total of 48 h before the migration of cancer cells towards the DRG was quantified as the nerve invasion index (α/γ), while the extension of DRG axons towards the prostate cancer colonies was evaluated by determining the DRG outgrowth index (β/γ).

Perineural invasion assay

A 3D co-culture model of cancer-nerve cell was established based on a previously published protocol with slight adjustment. PC-12 cells, a classical neuronal model, exhibit a phenotype akin to that of neurons following differentiation induced by NGF. After staining PC12 with Cell-Tracker Green CMFDA (Invitrogen, Thermo Fisher Scientific, Waltham, USA), 1×10^4 of PC12 were injected into 1.5 μL of Matrigel and added with 75 μM of Forskolin (Sigma-Aldrich, St. Louis, MO, USA) for 24 h in 6 well cell culture pool. After staining the tumor cell with Cell-Tracker Red CMTPX(Invitrogen, Thermo Fisher Scientific, Waltham, USA), they were inoculated around the matrix and cultured for 48 h. The cancer cells involved in PNI were visualized and photographed under a fluorescence microscope (Olympus Corporation, Tokyo, Japan). The vitro model of PNI was established by Transwell invasion assay. The Upper chamber was seeded with cancer cell; Lower chamber was seeded with PC12 cells. After 24 h, the upper surface cancer cell was cleaned. Cancer cells that had traversed the membrane was stained with 0.1% crystal violet, followed by visualization under a DMR inverted microscope (Leica Microsystems, Wetzlar, Germany).

In vivo model of PNI

The in vivo model of perineural invasion (PNI) was established following established procedures [56, 57]. At the age of four weeks, nude mice were anesthetized using isoflurane (Sigma-Aldrich, St. Louis, MO, USA), and the right sciatic nerve was surgically exposed. Prostate cancer cells were then microscopically injected into the vicinity of the sciatic nerve. A microinjection of 5 μL of a cell suspension containing 1×10^5 cells per microliter was performed using a 10 μL microsyringe. Over a duration of 7 weeks, the mice were monitored weekly for parameters including weight, tumor volume, sciatic nerve condition, and limb functionality. The index for assessing sciatic nerve function was calculated based on the distance between the first and fifth toes of the hind limbs. Limb function was graded by the hind limb paw response to manual extension, with a scale ranging from 4 (normal) to 1 (complete paw paralysis). All animal experiments were conducted in compliance with the ARRIVE guidelines.

RNA-sequencing and analysis

Total RNA was extracted from DU145 and PC-3 cells, with and without silenced PCDH12A, using the Trizol reagent (Invitrogen, Thermo Fisher Scientific, Waltham, MA, USA) following standard procedures. The mRNA-seq library was prepared. The library sequencing was performed, and the raw data were deposited. Differential expression analysis was performed using DESeq2. Genes with an absolute log2 fold change greather than 1 and FDR-adjusted p-value of less than 0.05 were considered significantly differentially expressed.

The DAVID database was utilized to perform GO enrichment analysis and KEGG pathway analysis to investigate the functions and potential signaling pathways of DEGs. KEGG pathway enrichment analysis was performed. The terms were significant enrichment with P-value < 0.05.

Co-immunoprecipitation (Co-IP) and mass spectrometry (MS)

Cells expressing Flag-tagged *FAM135A* or empty vector control were lysed. The lysates were incubated with Anti-Flag M2 Affinity Gel (Sigma-Aldrich). After extensive washing, bound proteins were eluted and subjected to tryptic digestion. The resulting peptides were analyzed by liquid chromatography-tandem mass spectrometry (LC-MS/MS). The raw data were processed and searched against the SwissProt human database.

Quantitative real-time polymerase chain reaction (qRT-PCR)

Total RNA was extracted using TRIzol reagent (Invitrogen, Thermo Fisher Scientific, Catalog # 15596026) according to the manufacturer's instructions. RNA concentration and purity were measured using a NanoDrop spectrophotometer. 1 μg of total RNA was reverse transcribed into cDNA using the PrimeScript RT Master Mix (TaKaRa, Catalog # RR036A). qRT-PCR was performed using TB Green Premix Ex Taq II (TakaRa, Catalog # RR820A) on a QuantStudio 5 Real-Time PCR System (Applied Biosystems). The amplification conditions were 95℃ for 30 s, 95℃ for 3 s, 60℃ for 30 s, 40 cycles. The

mRNA relative expression of target gene was calculated by $2^{-\triangle\triangle Ct}$ method.

Western blotting assay

Total proteins were acquired from the cells and lysed with RIPA (Beyotime Biotechnology, Shanghai, China). Total protein concentration was determined by BCA assay (Thermo Fisher Scientific, Waltham, MA, USA). 12% SDS-polyacrylamide gels were used to separated proteins by electrophoresis. The proteins were transferred to a PVDF membrane (Millipore Sigma, Burlington, MA, USA). Sealing membranes were blocked with 5% skim milk for 1 h at room temperature. Primary antibodies (Cell Signaling Technology, Danvers, USA) were incubated overnight at 4 °C; Membranes were washed three times with TBST (Sigma-Aldrich, St. Louis, MO, USA) for 5 min each. The secondary antibodies (Cell Signaling Technology, Danvers, USA) were incubated for 1 h at room temperature. The membrane was washed three times with TBST. The ECL luminescence solution was used for visualization. Image was used to analyze the relative expression of protein bands.

ChIP-qPCR assay

ChIP was performed using BersinBioTM Chromatin Immunoprecipitation (ChIP) Kit (BersinBio, Catalog Bes5001, Guangzhou, China) according to the manufacturer's protocol. Briefly, 2×10^7 cells were harvested for chromatin preparation. The cells were fixed with 1% formaldehyde ((Sigma-Aldrich, St. Louis, USA)) for 10 min at room temperature, washed twice with PBS, collected and resuspended in lysis buffer. The DNA was fragmented by sonication, and Anti-STAT3r IgG antibodies (Cell Signaling Technology, Danvers, USA) were added into lysate to generate the protein/DNA complexes. Finally, the complexes were reverse cross-linked to free immunoprecipitated DNA. ChIP-qPCR was performed using the QuantStudio™ Dx Real-Time PCR Instrument with SYBR green dye (Thermo Fisher Scientific, Waltham, MA, USA).

H&E staining

H&E staining (hematoxylin and eosin staining) is a commonly used histological and pathological staining technique, used to display cellular and tissue structures in tissue sections. Tissue sections are deparaffinized using xylene solvent (Sigma-Aldrich, St. Louis, MO, USA). Dehydration is carried out using different concentrations of ethanol. The section is then stained in hematoxylin stain for a duration of typically 5 min. Following hematoxylin staining, the section is differentiated using hydrochloric acid-ethanol solution. After differentiation, the section is rinsed with tap water and then stained in eosin solution. The stained section is dehydrated, followed by clearing in xylene. Finally, the section is cover-slipped with neutral resin to fix and increase transparency for observation and photography under a microscope.

Statistical analysis

The data is presented as the Mean ± Standard deviation (SD). Analysis of the in vivo data was conducted using GraphPad Prism software (version 8.2; Graphpad Software, Inc). Student's t-test (unpaired) was used for pairwise comparisons when there were 2 groups. For experiments with 3 groups, Dunnett's post hoc test in conjunction with one-way ANOVA was employed to compare the control group with the other groups. All statistical tests were two-sided, and a p-value < 0.05 was considered statistically significant.

Supplementary Information

The online version contains supplementary material available at https://doi.org/10.1186/s12943-025-02508-2.

Supplementary Material 1: Supplementary Figure 1.Silencing of ***FAM135A*** inhibits proliferation of prostate cancer tumor cells and induces cell death. A. ***FAM135A*** was silenced in prostate cancer cell lines DU145 and PC3, and the efficiency of gene silencing was verified by qRT-PCR; B. The knockdown efficiency was rigorously validated by Western blot. C. Silencing of ***FAM135A*** significantly inhibited the growth of prostate cancer cells; D-E. Clonogenic assays were used to test the effect of ***FAM135A*** silencing on the proliferation of PCa cells; F-G. Annexin V/PI double staining experiments revealed that silencing of ***FAM135A*** induced apoptosis in PCa cells.*** P<0.01; *** P<0.001;*.

Supplementary Material 2. Supplementary Figure 2. Knockdown of ***SRRM1*** or ***RNPS1*** does not affect the nuclear localization of FAM135A. (A) FAM135A is localized to the cell nucleus (scale bar: 10 μm)：data from The Human Protein Atlas database; (B) Flag tag was constructed for FAM135A, and potential binding proteins were identified through co-immunoprecipitation, with a focus on proteins involved in cytoplasmic-nuclear transport, resulting in the identification of proteins: SRRM1, RNPS1; (C) qRT-PCR analysis showing the mRNA expression levels of ***SRRM1*** in DU145 and PC3 cells after transfection with specific shRNAs; (D) Western blot analysis confirming the protein knockdown efficiency of ***SRRM1*** in DU145 and PC3 cells. (E) qRT-PCR analysis showing the mRNA expression levels of ***RNPS1*** in DU145 and PC3 cells after transfection with specific shRNAs.(F) Western blot analysis confirming the protein knockdown efficiency of ***RNPS1*** in DU145 and PC3 cells. (G) Western blot analysis of ***FAM135A*** protein levels in cytoplasmic (cFAM135A) and nuclear (nFAM135A) fractions from DU145 and PC3 cells after knockdown of ***SRRM1*** or ***RNPS1***. β-actin and PCNA serve as markers for cytoplasmic and nuclear fractions, respectively. Knockdown of ***SRRM1*** or ***RNPS1*** did not significantly alter the nuclear abundance of FAM135A.

Supplementary Material 3: Supplementary Figure 3. RNA-Seq and ChIP-Seq analysis reveals the impact of FAM135A on gene transcription regulation. A. Heatmap displaying differentially expressed genes in DU145 cells; B. Heatmap displaying differentially expressed genes in PC3 cells; C. Heatmap displaying genes with consistent differential expression trends in both DU145 and PC3 cells; D. ChIP-Seq results showing genes bound by FAM135A in DU145 and PC3 cells.

Supplementary Material 4: Supplementary Figure 4.Validation of ***TENM3*** knockdown efficiency. (A) qRT-PCR analysis showing the mRNA expression levels of ***TENM3*** in DU145 and PC3 cells after transfection with ***TENM3***-specific shRNA. (B) Western blot analysis confirming the reduction of TENM3 protein levels in DU145 and PC3 cells after ***TENM3*** knockdown. GAPDH serves as a loading control.*Data are presented as mean± SD; **p < 0.001.

Supplementary Material 5: Supplementary Figure5. RT-qPCR assay confirming the successful overexpression of ***TENM3*** protein in DU145 and PC3 cells that had been stably transduced with shFAM135A or control shRNA (shNC). GAPDH serves as a loading control. This demonstrates the establishment of the rescue cell models (shFAM135A + Vector vs. shFAM135A + TENM3-OE) used in the functional experiments shown in Figure 7. **** Indicates comparison with the NC group,*P<0.05; **P<0.01; ***P<0.001; # indicates comparison with the shFAM135A group, #P<0.05; ##P<0.01; ###P<0.001***.

Supplementary Material 6: Supplementary Figure 6. Correlation analysis of ***FAM135A*** expression with neuroactive ligand-receptor pairs in PNI vs. Non-PNI prostate cancer samples. Scatter plots showing the expression correlation between ***FAM135A*** and each of the ten significantly differential neuroactive ligand-receptor genes. Pearson correlation coefficient (R) and p-value are indicated for each pair.

Supplementary Material 7.

Supplementary Material 8.

Acknowledgements
None.

Authors' contributions
N.Z, X.R, and R.N made substantial contributions to the conception and design of the work; N.Z, X.R, S.C, R.S, X.Y, C.Y, and S.A performed the experiments; X.R, Y.Z, S.C, and R.N performed analysis and interpreted the data; N.Z, X.R, and R.N drafted the work; B.S.H, A.T.N, R.K.L, and R.N revised and provided comments on the work. All authors reviewed the manuscript.

Funding
This work was supported by (1) Shenzhen-Hong Kong-Macau Science and Technology Program (Category C; SGDX20220530111403024), and Seed Fund for PI Research-Basic Research (2402101653) to Dr. Rong Na; (2) Guangci-Jinguang Innovation Project Launch Plan (GCQH2024091), the Shanghai "Rising Stars of Medical Talents" Youth Development Program (SHWSRS(2023)_62), the Joint Program on Health Science & Technology Innovation of Hainan Provincial (WSJK2025QN010), the Hainan Provincial Natural Science Foundation of China (825MS203) for Ning Zhang. All the funders had no role in study design, data collection, data analysis, interpretation, decision to publish, or preparation of the manuscript.

Data availability
No datasets were generated or analysed during the current study.

Declarations

Ethics approval and consent to participate
This study is approved by the Institutional Review Board at Ruijin Hospital, Shanghai (2022 – 128) and animal ethics (24–382) at The University of Hong Kong.

Consent for publication
All authors read and approved the final version of the manuscript. All authors read and approved the final manuscript.

Competing interests
The authors declare no competing interests.

Author details
[1]Department of Urology, Ruijin Hospital, Shanghai Jiao Tong University School of Medicine, Shanghai, China
[2]Department of Urology, Renji Hospital, Shanghai Jiao Tong University School of Medicine, Shanghai, China
[3]Department of Pathology, Ruijin Hospital, Shanghai Jiao Tong University School of Medicine, Shanghai, China
[4] Division of Urology, Department of Surgery, LKS Faculty of Medicine, The University of Hong Kong, Hong Kong, China
[5]Division of Urology, Department of Surgery, Queen Mary Hospital, Hong Kong, China
[6]Division of Urology, Department of Surgery, The University of Hong Kong Shenzhen Hospital, Shenzhen, Guangdong, China

Received: 18 July 2025 / Accepted: 16 October 2025
Published online: 17 November 2025

References

1. Siegel RL, Miller KD, Wagle NS, Jemal A. Cancer statistics, 2023. CA Cancer J Clin. 2023;73:17–48.
2. Rebello RJ, Oing C, Knudsen KE, Loeb S, Johnson DC, Reiter RE, et al. Prostate cancer. Nat Rev Dis Primers. 2021;7:9.
3. Desai K, McManus JM, Sharifi N. Hormonal therapy for prostate cancer. Endocr Rev. 2021;42:354–73.
4. Cheng Q, Butler W, Zhou Y, Zhang H, Tang L, Perkinson K, et al. Pre-existing castration-resistant prostate cancer-like cells in primary prostate cancer promote resistance to hormonal therapy. Eur Urol. 2022;81:446–55.
5. Winkler F, Venkatesh HS, Amit M, Batchelor T, Demir IE, Deneen B, Gutmann DH, Hervey-Jumper S, Kuner T, Mabbott D, Platten M, Rolls A, Sloan EK, Wang TC, Wick W, Venkataramani V. Monje, cancer neuroscience: state of the field, emerging directions. Cell. 2023;186:1689–707.
6. Prillaman M. How cancer hijacks the nervous system to grow and spread. Nature. 2024;626:22–4.
7. Anastasaki C, Gao Y, Gutmann DH. Neurons as stromal drivers of nervous system cancer formation and progression. Dev Cell. 2023;58:81–93.
8. Pan C, Winkler F. Insights and opportunities at the crossroads of cancer and neuroscience. Nat Cell Biol. 2022;24:1454–60.
9. Keough MB, Monje M. Neural signaling in cancer. Annu Rev Neurosci. 2022;45:199–221.
10. Niu Y, Forster S, Muders M. The role of perineural invasion in prostate cancer and its prognostic significance. Cancers (Basel). 2022. https://doi.org/10.3390/cancers14174065.
11. Teramoto Y, Wang Y, Miyamoto H. Risk stratification by quantification of perineural cancer invasion on prostate needle core biopsy: should it be counted? J Urol. 2023;210:639–48.
12. Hou Y, Lin B, Xu T, Jiang J, Luo S, Chen W, et al. The neurotransmitter calcitonin gene-related peptide shapes an immunosuppressive microenvironment in medullary thyroid cancer. Nat Commun. 2024;15:5555.
13. Fu Y, Shen K, Wang H, Wang S, Wang X, Zhu L, et al. Alpha5 nicotine acetylcholine receptor subunit promotes intrahepatic cholangiocarcinoma metastasis. Signal Transduct Target Ther. 2024;9:63.
14. Cao Y, Ge X, Zhu X, Han Y, Wang P, Akakuru OU, et al. Transformable neuropeptide prodrug with tumor microenvironment responsiveness for tumor growth and metastasis inhibition of Triple-Negative breast cancer. Adv Sci. 2023;10:e2300545.
15. Padmanaban V, Keller I, Seltzer ES, Ostendorf BN, Kerner Z, Tavazoie SF. Neuronal substance P drives metastasis through an extracellular RNA-TLR7 axis. Nature. 2024;633:207–15.
16. Lu C, Mahajan A, Hong SH, Galli S, Zhu S, Tilan JU, Abualsaud N, Adnani M, Chung S, Elmansy N, Rodgers J, Rodriguez O, Albanese C, Wang H, Regan M, Zgonc V, Blancato J, Krawczyk E, Gallicano GI, Girgis M, Cheema A, Izycka-Swieszewska E, Cavalli LR, Pack SD, Kitlinska J. Hypoxia-activated neuropeptide Y/Y5 receptor/RhoA pathway triggers chromosomal instability and bone metastasis in ewing sarcoma. Nat Commun. 2022;13:2323.
17. Wang J, Wei J, Pu T, Zeng A, Karthikeyan V, Bechtold B, Vo K, Chen J, Lin TP, Chang AP, Corey E, Puhr M, Klocker H, Culig Z, Bland T, Wu BJ. Cholinergic signaling via muscarinic M1 receptor confers resistance to docetaxel in prostate cancer, cell reports. Medicine. 2024;5:101388.
18. Liu YN, Liu MK, Wen YC, Li CH, Yeh HL, Dung PVT, et al. Binding of interleukin-1 receptor antagonist to cholinergic receptor muscarinic 4 promotes immunosuppression and neuroendocrine differentiation in prostate cancer. Cancer Lett. 2024;598:217090.
19. Shi DD, Guo JA, Hoffman HI, Su J, Mino-Kenudson M, Barth JL, Schenkel JM, Loeffler JS, Shih HA, Hong TS, Wo JY, Aguirre AJ, Jacks T, Zheng L, Wen PY, Wang TC, Hwang WL. Therapeutic avenues for cancer neuroscience: translational frontiers and clinical opportunities. Lancet Oncol. 2022;23:e62–74.
20. Huang D, Alexander PB, Li QJ, Wang XF. GABAergic signaling beyond synapses: an emerging target for cancer therapy. Trends Cell Biol. 2023;33:403–12.
21. Chen ZF. A neuropeptide code for itch. Nat Rev Neurosci. 2021;22:758–76.

22. Kanehisa K, Koga K, Maejima S, Shiraishi Y, Asai K, Shiratori-Hayashi M, et al. Neuronal pentraxin 2 is required for facilitating excitatory synaptic inputs onto spinal neurons involved in pruriceptive transmission in a model of chronic itch. Nat Commun. 2022;13:2367.
23. Sheahan TD, Warwick CA, Cui AY, Baranger DAA, Perry VJ, Smith KM, et al. Kappa opioids inhibit spinal output neurons to suppress itch. Sci Adv. 2024;10:eadp6038.
24. Li H, Chen X, Xu J, Zhu L, Li C, Sun X, et al. GRP/GRPR enhances alcohol-associated liver injury through the IRF1-mediated Caspase-1 inflammasome and NOX2-dependent ROS pathway. Hepatology. 2024;79:392–408.
25. Li C, Ma QY, Liu XQ, Li HD, Yu MJ, Xie SS, et al. Genetic and pharmacological inhibition of GRPR protects against acute kidney injury via attenuating renal inflammation and necroptosis. Mol Ther. 2023;31:2734–54.
26. Goto F, Kiyama Y, Ogawa I, Okuno H, Ichise T, Ichise H, et al. Gastrin-releasing peptide regulates fear learning under stressed conditions via activation of the amygdalostriatal transition area. Mol Psychiatry. 2022;27(3):1694–703.
27. Kayalar O, Oztay F, Ongen HG. Gastrin-releasing peptide induces fibrotic response in MRC5s and proliferation in A549s, cell communication and signaling. CCS. 2020;18:96.
28. Peng S, Zhan Y, Zhang D, Ren L, Chen A, Chen ZF, et al. Structures of human gastrin-releasing peptide receptors bound to antagonist and agonist for cancer and itch therapy. Proc Natl Acad Sci U S A. 2023;120:e2216230120.
29. Chen L, Zhang J, Chi C, Che W, Dong G, Wang J, et al. Lower-grade gliomas surgery guided by GRPR-targeting PET/NIR dual-modality image probe: a prospective and single-arm clinical trial. Theranostics. 2024;14:819–29.
30. Wang W, Wu KJ, Vellaisamy K, Leung CH, Ma DL. Peptide-conjugated long-lived theranostic imaging for targeting GRPr in cancer and immune cells. Angew Chem Int Ed Engl. 2020;59:17897–902.
31. Duan H, Moradi F, Davidzon GA, Liang T, Song H, Loening AM, Vasanawala S, Srinivas S, Brooks JD, Hancock S, Iagaru A. (68)Ga-RM2 PET-MRI versus MRI alone for evaluation of patients with biochemical recurrence of prostate cancer: a single-centre, single-arm, phase 2/3 imaging trial, the lancet. Oncology. 2024;25:501–8.
32. Sollini M, Calais J, Chiti A, Emmett L, Fanti S, Fendler W, Herrmann K, Hope TA, Sartor O, Shuch B, Tagawa S, Hofman MS. Novel Radiopharmaceuticals and Future of Theranostics in Genitourinary Cancers, European urology. 2024.
33. Nisman B, Oleinikov K, Nechushtan H, Maimon O, Atlan K, Peled N, Gross D, Peretz T, Meirovitz A. Grozinsky-Glasberg, plasma Progastrin-Releasing peptide and chromogranin A assays for diagnosing and monitoring lung Well-Differentiated neuroendocrine tumors: A brief report. J Thorac Oncology: Official Publication Int Association Study Lung Cancer. 2023;18:369–76.
34. Bakker IL, Froberg AC, Busstra MB, Verzijlbergen JF, Konijnenberg M, van Leenders G, Schoots IG, de Blois E, van Weerden WM, Dalm SU, Maina T, Nock BA, de Jong M. GRPr antagonist (68)Ga-SB3 PET/CT imaging of primary prostate cancer in Therapy-Naive Patients, journal of nuclear medicine: official publication. Soc Nuclear Med. 2021;62:1517–23.
35. Schollhammer R, Robert G, Asselineau J, Yacoub M, Vimont D, Balamoutoff N, et al. Comparison of (68)Ga-PSMA-617 PET/CT and (68)Ga-RM2 PET/CT in patients with localized prostate cancer who are candidates for radical prostatectomy: a prospective, single-arm, single-center, phase II study. journal of nuclear medicine: official publication Soc Nuclear Med. 2023;64:379–85.
36. Xu J, Hu M, Gao Y, Wang Y, Yuan X, Yang Y, et al. LncRNA MIR17HG suppresses breast cancer proliferation and migration as CeRNA to target FAM135A by sponging miR-454-3p. Mol Biotechnol. 2023;65:2071–85.
37. Lou X, Ye Z, Xu X, Jiang M, Lu R, Jing D, et al. Establishment and characterization of the third non-functional human pancreatic neuroendocrine tumor cell line. Hum Cell. 2022;35:1248–61.
38. Prueitt RL, Yi M, Hudson RS, Wallace TA, Howe TM, Yfantis HG, et al. Expression of MicroRNAs and protein-coding genes associated with perineural invasion in prostate cancer. Prostate. 2008;68:1152–64.
39. Yang Y, Guo L, Chen L, Gong B, Jia D, Sun Q. Nuclear transport proteins: structure, function, and disease relevance. Signal Transduct Target Ther. 2023;8:425.
40. El-Tanani M, Nsairat H, Mishra V, Mishra Y, Aljabali AAA, Serrano-Aroca A, et al. Ran GTPase and its importance in cellular signaling and malignant phenotype. Int J Mol Sci. 2023. https://doi.org/10.3390/ijms24043065.
41. Fukuchi J, Hiipakka RA, Kokontis JM, Hsu S, Ko AL, Fitzgerald ML, et al. Androgenic suppression of ATP-binding cassette transporter A1 expression in LNCaP human prostate cancer cells. Cancer Res. 2004;64:7682–5.
42. Lee BH, Taylor MG, Robinet P, Smith JD, Schweitzer J, Sehayek E, et al. Dysregulation of cholesterol homeostasis in human prostate cancer through loss of ABCA1. Cancer Res. 2013;73:1211–8.
43. Hiwatari M, Seki M, Matsuno R, Yoshida K, Nagasawa T, Sato-Otsubo A, et al. Novel TENM3-ALK fusion is an alternate mechanism for ALK activation in neuroblastoma. Oncogene. 2022;41:2789–97.
44. Saidi A, Stallons TA, Wong AG, Torgue JJ, Society of Nuclear Medicine. Preclinical investigation of [(212)Pb]Pb-DOTAM-GRPR1 for peptide receptor radionuclide therapy in a prostate tumor model. J Nucl Med. 2024. https://doi.org/10.2967/jnumed.124.268101.
45. Liu X, Wang Y, Tao T, Zeng L, Wang D, Wen Y, et al. GRPR/extracellular signal-regulated kinase and NPRA/extracellular signal-regulated kinase signaling pathways play a critical role in spinal transmission of chronic itch. J Invest Dermatol. 2021;141:863–73.
46. Jin F, Irshad S, Yu W, Belakavadi M, Chekmareva M, Ittmann MM, et al. ERK and AKT signaling drive MED1 overexpression in prostate cancer in association with elevated proliferation and tumorigenicity, molecular cancer research. MCR. 2013;11:736–47.
47. Liu Q, Ma Z, Cao Q, Zhao H, Guo Y, Liu T, et al. Perineural invasion-associated biomarkers for tumor development. Biomed Pharmacother. 2022;155:113691.
48. Yin L, Li J, Wang J, Pu T, Wei J, Li Q, et al. *MAOA* promotes prostate cancer cell perineural invasion through *SEMA3C*/PlexinA2/*NRP1*-cMET signaling. Oncogene. 2021;40:1362–74.
49. Harada N, Ohmori Y, Yamaji R, Higashimura Y, Okamoto K, Isohashi F, et al. ARA24/Ran enhances the androgen-dependent NH2- and COOH-terminal interaction of the androgen receptor. Biochem Biophys Res Commun. 2008;373:373–7.
50. Berns DS, DeNardo LA, Pederick DT, Luo L. Teneurin-3 controls topographic circuit assembly in the hippocampus. Nature. 2018;554:328–33.
51. Hunyara JL, Daly KM, Torres K, Yurgel ME, Komal R, Hattar S, et al. Teneurin-3 regulates the generation of non-image-forming visual circuitry and responsiveness to light in the suprachiasmatic nucleus. PLoS Biol. 2023;21:e3002412.
52. Li XC, Wang MY, Yang M, Dai HJ, Zhang BF, Wang W, et al. A mutational signature associated with alcohol consumption and prognostically significantly mutated driver genes in esophageal squamous cell carcinoma. Ann Oncol. 2018;29:938–44.
53. Zaret KS, Carroll JS. Pioneer transcription factors: establishing competence for gene expression. Genes Dev. 2011;25:2227–41.
54. Su N, Wang Y, Qian M, Deng M. Combinatorial regulation of transcription factors and microRNAs. BMC Syst Biol. 2010;4:150.
55. Lee JT, Lee S, Yun CJ, Jeon BJ, Kim JM, Ha HK, et al. Prediction of perineural invasion and its prognostic value in patients with prostate cancer. Korean J Urol. 2010;51:745–51.
56. Zheng S, Hu C, Lin Q, Li T, Li G, Tian Q, et al. Extracellular vesicle-packaged PIAT from cancer-associated fibroblasts drives neural remodeling by mediating m5C modification in pancreatic cancer mouse models. Sci Transl Med. 2024;16:eadi0178.
57. Zhang W, He R, Yang W, Zhang Y, Yuan Q, Wang J, et al. Autophagic Schwann cells promote perineural invasion mediated by the NGF/ATG7 paracrine pathway in pancreatic cancer. J Exp Clin Cancer Res. 2022;41:48.

Publisher's Note